Design of a Wearable to Improve Single-Device Motion Classification of Arm Motions

by

Jordan David Chun Yuu Lui

B.A.Sc, University of Waterloo, 2013

Thesis Submitted in Partial Fulfillment of the
Requirements for the Degree of
Master of Applied Science

in the
School of Engineering Science
Faculty of Applied Science

SIMON FRASER UNIVERSITY
Fall 2019

Approval

Name:	**Jordan David Chun Yuu Lui**
Degree:	**Master of Applied Science (Biomedical Engineering)**
Title:	**Design of a Wearable to Improve Single-Device Motion Classification of Arm Motions**
Examining Committee:	**Chair: Atousa Hajshirmohammadi** Lecturer
	Carlo Menon P.Eng Senior Supervisor Professor
	Mirza Faisal Beg Supervisor Professor
	Mohammad Narimani Internal Examiner Lecturer
Date Defended/Approved:	November 26, 2019

Ethics Statement

The author, whose name appears on the title page of this work, has obtained, for the research described in this work, either:

a. human research ethics approval from the Simon Fraser University Office of Research Ethics

or

b. advance approval of the animal care protocol from the University Animal Care Committee of Simon Fraser University

or has conducted the research

c. as a co-investigator, collaborator, or research assistant in a research project approved in advance.

A copy of the approval letter has been filed with the Theses Office of the University Library at the time of submission of this thesis or project.

The original application for approval and letter of approval are filed with the relevant offices. Inquiries may be directed to those authorities.

Simon Fraser University Library
Burnaby, British Columbia, Canada

Update Spring 2016

Abstract

Inertial Measurement Unit (IMU) based wearable sensors have found common use to track arm activity in daily life. However, classifying a high number of arm motions with single IMU-based systems remains a challenging task. In this study, we propose a single-device wearable which incorporates a thermal sensor and an inertial sensor. The system was evaluated in a study incorporating 11 healthy participants, where 24 different arm motions were recorded and predicted with a machine learning classifier. This study found that 24 arm motions could be classified with 93.55% accuracy. Further, the passive infrared thermal sensor significantly increased classification accuracy from 75% to 93.55% , p=<0.05. The performance of the generalized classifier indicates that the device could classify arm motions on a user without prior training.

Keywords: Motion classification; rehabilitation devices; physical rehabilitation; stroke rehabilitation; rehabilitation wearable; human activity recognition, human motion classification, motion classification

Acknowledgements

I thank everyone in the MENRVA lab, my parents, my sister, and my wife.

Table of Contents

List of Tables

List of Figures

List of Acronyms

AOA	Angle of Arrival
AC	Alternating Current
DC	Direct Current
FOV	Field of View
GPS	Global Positioning System
IMU	Inertial Measurement Unit
IR	Infrared
LOOCV	Leave-one-out cross validation
LPF	Low Pass Filter
PIR	Passive Infrared
PSD	Power Spectrum Density
RSS	Received Signal Strength
TDOA	Time Difference of Arrival
TOA	Time of Arrival
VLP	Visible Light Positioning

Glossary

EEG	Electroencephalography (EEG) is the measure of a neural signals. These neural signals can be acquired using electrodes which are either placed on the surface of the scalp or implanted. The signal readings can vary with brain activity (thinking, sleeping, moving limb, etc.) These signal measurements can be used as an input to a Brain Computer Interface (BCI) [1]
EMG	Electromyography (EMG) is the measure of electric potential that occurs due to muscle activation [2].
Galvanic Skin Response	A measurement of electrical properties (resistance) at the surface of the skin. These properties can change in relation to environmental stimuli and changes in an emotional state [3]
RFID	Radiofrequency Identification. The signal strength of a connection between RFID device and an RFID reader can indicate proximity, and this can be used to sense the presence of a user or sense interaction with the environment [3]

Chapter 0.

Disclaimer on previous publication of work

0.1. Prior publication of content

The material of this thesis is excerpted, modified, and reproduced with permissions from the following papers which were published in peer-reviewed journals:

Lui J, Menon C. Would a thermal sensor improve arm motion classification accuracy of a single wrist-mounted inertial device?. Biomedical engineering online. 2019 Dec;18(1):53

Lui, J, Vegni AM, Colace L, Menon C, Neri A. Preliminary design and characterization of a low-cost and low-power visible light positioning system., Applied Optics, 2018

The material of this thesis is excerpted, modified, reproduced with permission. Sections have been adapted from the work above to fit the scope and formatting of the thesis. Text and figures reproduced in this thesis do not reference the above-mentioned papers for the sake of clarity.

0.2. Contributions to this thesis

Contributions strictly related to the thesis and hereafter presented are the following:

Lui J, Menon C. Would a thermal sensor improve arm motion classification accuracy of a single wrist-mounted inertial device?. Biomedical engineering online. 2019 Dec;18(1):53.

Lui J, Ferrone A, Andrews K, Colace L, Menon C. A preliminary investigation into infrared sensors in wearables for upper extremity motion sensing. Future Technologies Conference. 2017. p. 120–5.

Other works published during my MASc degree which are not part of my thesis but assisted me to acquire related knowledge in the field of optical wearable device design include the following:

Lui, J, Vegni AM, Colace L, Menon C, Neri A. Preliminary design and characterization of a low-cost and low-power visible light positioning system., Applied Optics, 2018

Lui J, Ferrone A, Lim ZY, Colace L, Menon C. A Novel Wearable for Rehabilitation Using Infrared Sensors: A Preliminary Investigation. International Work-Conference on Bioinformatics and Biomedical Engineering. 2017. p. 573–83.

Lui, J, Vegni AM, Colace L, Menon C, Neri A. Toward an Experimental Testbed for RSS-based Indoor Visible Light Positioning. IEEE COMSOC MMTC Communications – Frontiers. 2017. Vol 12. No 3. P 19-22

Lui J, Naylor A, Zhou M, Khoshnam M, Chhatre N, Mahanfar A, Menon C. Monitoring Upper-Limb Activity Based on Radio Frequency Time-of-Flight Distance Measurement. In 2018 IEEE 9th Annual Information Technology, Electronics and Mobile Communication Conference (IEMCON) 2018 Nov 1 (pp. 54-60). IEEE.

Chapter 1.

Introduction

This chapter begins by outlining the motivation for this thesis. Subsequently, the objectives of this thesis are defined. Finally, a layout of the thesis chapters is provided.

1.1. Motivation

The tracking of human motion is of interest to several fields including the medical, rehabilitation, sports, military, and security industries [4][5]. Despite its potentially significant impact, the ability to track human motion using single wearable devices has been difficult.

The availability of accurate and efficient wearable sensors has been particularly important in the medical and rehabilitation fields. With the aging population, there is an increased need for detecting health events such as freezing in the gait cycle of Parkinson's patients, epileptic seizures, and fall detection [6]. Wearable sensors also find application in cognitive function assessment, physical activity monitoring [7], sleep quality monitoring [8], and exercise classification for stroke survivors [9].

Patients typically begin their physical rehabilitation in a clinical environment, and may transition to home-based rehabilitation (HBR). HBR is an important component of the patient's recovery because it allows a continuation of treatment after clinical discharge. HBR can contribute to an increased degree of functional recovery [10].

HBR is also an important component of patient rehabilitation because some patients are not comfortable exercising in a clinical environment, and some patients have difficulty physically accessing a clinical location [11]. Thus, HBR rehabilitation can be

completed in a location that is accessed more conveniently. HBR has strong potential for helping to improve health outcomes but a key challenge exists: patients have difficulty adhering to the regimen and difficulty reporting accurately on their exercise progress [12],[13]. These issues in self-reporting on HBR could be mitigated by exercise monitoring systems.

Some systems exist for monitoring patient exercise at home. These systems usually track motion through the use of either camera vision systems placed in the room [14] or via body-worn sensors (wearables). Vision systems, however, present privacy concerns [15]. Further, vision-based systems are only usable in a single room. Wearable sensor systems instead utilize on-body sensors to classify human motion and can be used in multiple locations. Most of the wearable systems presented for classifying arm motions require sensors to be worn on multiple limbs; these systems present a barrier to usage because they are more difficult to don than single-device systems.

Challenges of the existing vision systems and multi-device sensor systems indicate that the current solutions do not obviate the need for a simple and accurate system for the tracking of exercise during HBR. A clear solution to the issue is to develop a single device wearable sensor system which can accurately track arm motions. Such a system would address the challenges of the existing systems and would also be easier to don and configure. This is particularly important for rehabilitation where the stamina of the user might be limited by their condition.

A literature review of single-device based systems for arm motion classification identified studies where up to 6 arm motions were classified. This low number of classified motions is arguably due to a difficulty in classifying higher numbers of arm motions with a single inertial sensor. Detecting multiple arm motions could be useful for patients

undergoing physical rehabilitation. In the example of stroke survivors, rehabilitation exercise manuals such as Chedoke-McMaster Stroke Assessment [16], Chedoke Arm and Hand Activity Inventory (CAHAI) [17], and Graded Repetitive Arm Supplementary Program (GRASP) [18] each protocol lists more than 6 motions, and therefore it is imperative to explore other solutions that can realize classification of higher numbers of arm movements. Incorporating additional sensor data might improve the classification performance of single-device systems. Increasing the number of motions that can be tracked could improve the applicability of these wearables for home-based rehabilitation, which is an attractive alternative to clinical rehabilitation when treatment inaccessibility is a noted obstacle to accessing treatment [11][9].

Some studies have indicated that the use of optical sensors could provide valuable information for sensing human activity in an indoor environment [19] [20] [21] [22] [23]. These studies demonstrate some capability for optical sensors to classify user position in room and ambulation (walking) activities. However, no studies were found to investigate the classification of user arm motions using an optical sensor. It is possible that introducing an optical sensor into a single-device system might increase the performance of an activity classifier, and possibly increase the number of arm motions that can be classified.

If the sensor is fixed on a limb, such as an arm, it is possible that some information relating to motion could be gathered. The presence of heat sources in the environment could allow the arm's orientation to be determined relative to a stationary heat source. Additionally, the user themselves would be a heat source that is visible to the pyroelectric sensor. Seeing the user in the sensor Field of View (FOV) would provide some information about the relative orientation between the sensor-mounted limb and the body. Since the thermal sensor provides very different sensor data compared to conventional motion classification sensors (acceleration and rotation data from the accelerometers and

gyroscopes), the different sensor data could possibly augment classifier performance. An improved classification performance might result in a higher classification accuracy, a higher number of classified motions, or some improvement in the sensitivity of the classifier.

In summary, several studies of activity recognition have employed inertial sensors as their sole or primary sensor for motion classification. Notably, some studies have introduced light infrared sensors into wearable devices to classify ambulation activities. These studies, however, have not examined the feasibility of using a thermal sensor for arm motion classification. Additionally, the performance contribution of the thermal sensor has not been quantified. Therefore, there is a lack of literature describing the performance of infrared sensors in single-device arm motion classification wearable systems.

A device should be developed with the intention of increasing the number of arm motions that can be classified with a single-device system. A feasibility investigation of this proposed device should be performed in a controlled environment before it is used in unsupervised exercise monitoring environments. A controlled environment should have a supervisor present to monitor the usage of the device. The controlled environment should also situate the participant where other human heat sources will not interfere with the operation of the device's thermal sensor.

1.2. Thesis Objectives

Current single-device arm motion classification systems identified in literature can classify a maximum of 6 arm motions. This thesis aims to develop a system that can classify more than 6 motions. It is hypothesized that the incorporation of an infrared thermal sensor will increase the performance of a single-device wearable arm motion classification. This thesis consists of three main objectives:

Objective 1 is to develop a single-device arm motion classification system to classify a larger number of arm motions than prior systems identified in the literature.

Objective 2 is to perform a preliminary investigation on the performance of the system in a study of 24 arm motions, with healthy volunteers, in a controlled environment.

Objective 3 is to perform a preliminary investigation on the performance contribution of the thermal sensor, with healthy volunteers, in a controlled environment.

1.3. Thesis Layout

The chapters are organized as follows. The literature review is presented in Chapter 2, System design is described in Chapter 3, Experimental setup and methods are presented in Chapter 4, Results from the study are shared in Chapter 5 and Chapter 6, and the findings are concluded in Chapter 7.

Chapter 2.

Background

This section presents a background that is relevant to the thesis. Human motion classification is discussed first, including elaboration on raw data, data pre-processing, feature extraction, and classification. Following this, a review of related work in activity classification is presented.

2.1. Motion Classification

Human activity recognition (HAR) can be divided into two main sub-topics: posture classification, and motion classification. Posture classification refers to differentiating static orientations of the human body. Examples of postures include sitting, standing, and lying down [6][24].

Motion classification or movement classification refers to differentiating non-static activities [6]. Examples of motions include running, walking, opening a door, and picking up a phone.

Motion classification can be accomplished through subjective means such as diaries and questionnaires, however, this can lead to inconsistent results [6][13]. Motion can also be classified by objective means, typically employing simple mechanical devices, motion capture vision systems, or wearable devices. Mechanical devices like switches and goniometers can provide a quantitative measure of activity or joint angle [24]. Motion capture vision systems determine the position of the joints and limbs through the use of optical markers; this information can be analyzed to study pose and segmented to classify

activities. Wearable devices are mounted on the body and quantify the degree of movement, count steps taken, or classify the motions performed by a user [6].

Tracking physical activity is useful since decreased activity level can be related to illness and functional impairment [6]. Motion classification has become increasingly important, particularly in the area of at-home rehabilitation, where patients conduct exercises at home without supervision by medical personnel. The independence of such rehabilitation requires some means to accurately determine if the exercises were performed correctly. One method to evaluate these exercises is through the use of wearable devices. Motion classification and activity recognition via sensor technology can be described in several high level topics (Figure 2.1), as per Bulling et al [3]: Raw data acquisition, data pre-processing, data segmentation, feature extraction, and motion classification.

Table 2.1. Aspects of Human Activity Recognition [3]

Aspect of Activity Recognition	**Description**
Raw data acquisition	Extraction of data from sensors located on the device
Data pre-processing	Isolating the activity of interest in a continuous stream of activity. Note that this is outside of the scope of the thesis objectives

Data segmentation	Isolating the activity of interest in a continuous stream of activity. Note that this is outside of the scope of the thesis objectives
Feature extraction	Calculating secondary features from raw sensor data to increase the performance of the classifier
Classification	Determining which activity occurred

Figure 2.1. Stages of data processing in Activity Recognition. [3]

2.1.1. Raw Data

A variety of different sensor technologies have been used for human activity recognition, but inertial sensors (accelerometer, gyroscope, and magnetometer sensors) continue to be the most frequently used sensor solutions. Other sensor modalities that have been reported include pressure sensors [4], galvanic skin response [6], skin temperature [6], light sensors [19], EMG [25], EEG [26], GPS [27], and RFID [28]. Inertial

and optical sensors will be discussed below as they specifically pertain to the motivations of this thesis.

2.1.1.1 Inertial sensing systems

Inertial sensing systems classify human motion by recording the changes in orientation, force, and speed of the limb or body in motion. These systems frequently incorporate accelerometers, gyroscope, and magnetometers sensors [29]. Combined sensing units are often employed and are referred to as inertial measurement units (IMUs). Accelerometers and gyroscopes are some of the most commonly used sensor types in human motion sensing and classification studies.

An accelerometer measures linear acceleration across its axes; a gyroscope measures angular motion about its axes [6]. The two main types of accelerometer sensors are piezoresistive and differential capacitor sensors. Gyroscope sensors work by measuring the rate of angular displacement about each sensor axis [30]. Magnetometers are essentially a small digital compass, which sense the strength of the gravitational field vector relative to each sensor axis [31]. The magnetometer signal can be combined with the accelerometer value to locate the orientation of the sensor with respect to the Earth's orientation frame.

2.1.1.1.1 Inertial sensor frame of reference

Inertial sensing systems report their sensor measurements in a local frame of reference, commonly referred to as the body frame. This frame of reference differs from the other reference frames such as the Earth reference frame, room reference frame (often called navigation frame), and the inertial frame by a 3D transformation.

The magnetometer sensor measures the relative orientation between the IMU sensor's body frame and the Earth's magnetic north vector.

Accelerometer sensors measure force vector in the body frame (denoted by superscript 'B'). This can be represented as the vector subtraction of the linear acceleration in the navigation frame (denoted by superscript 'N') and the Earth gravity vector. The rotation matrix to transform from the navigation frame to the body frame is represented by R^{BN}. f^B denotes the force in the body frame, while a^N represents the acceleration in the navigation frame and g^N represents the force of gravity.

$$f^B = R^{BN}a^N - R^{BN}g^N \quad (1)$$

Gyroscope sensors measure the angular velocity (rate of change of orientation) of the body frame with respect to the inertial frame (ω_{IB}^B). Note that this angular velocity data in the body frame is expressed as being composed of three components: an angular rotation between inertial and Earth frame ω_{IE}^N, rotation between navigation and Earth frame ω_{EN}^N, and a rotation between the navigation and body frame ω_{NB}^B [32].

$$\omega_{IB}^B = R^{BN}\omega_{IE}^N + R^{BN}\omega_{EN}^N + \omega_{NB}^B \quad (2)$$

Inertial sensor data are then used for sensing orientation or position of a limb on which the sensor is mounted. In orientation sensing, the IMU sensor data can be used to determine the orientation of the person's limb in the body frame. This orientation in the body frame can be transformed into orientation in the navigation frame through matrix multiplication.

If a starting orientation of the body frame is established, changes in the body frame orientation are obtained by integrating the measured changes in angular velocity. The integration of angular velocity would yield an angular rotation estimate which can be used to update device orientation.

If the orientation of the sensor is determined in the body frame, the orientation in the navigation frame would be found via matrix multiplication.

$$R^N = R^B R^{BN} \tag{3}$$

Orientation in the navigation frame is more useful for functional interpretation of a person's movement, such as determining if the user's arm is raised upwards or downwards. Determining the orientation of the body relative to the room's reference frame could be used to determine an arm gesture or motion.

Data from the IMU can also be used to determine the position in 3D space through double integration of acceleration data, since the second integration of acceleration will yield a displacement value. The acceleration in the 3 different axes can be used to find the orientation of the sensor relative to the gravity vector, and this transformation can be used to determine the linear acceleration in 3 axes of the room's reference frame. These acceleration readings in 3 axes can be double integrated to obtain displacement readings at each timestep of measurement. This is referred to as dead reckoning [33].

Performing accurate and robust dead reckoning over a long period of time is difficult because small biases in accelerometer values are integrated and result in large scale errors over any longer period of time. An acceleration sensor with a small sensor bias may produce a small but non-zero value when the device is at rest. This small acceleration value will still result in a calculated displacement value at each time interval, causing the estimated position to drift over time.

Note that gyroscope data are often used to help determine if the device is at rest, which help to reduce the drift issues [34] that often negatively affect dead reckoning

algorithms. Combining data from different sensors to increase overall robustness is referred to as sensor fusion.

2.1.1.1.2 Inertial sensors in activity recognition

Inertial sensors can be used in motion classification when a recorded data stream is segmented and fed into an appropriate algorithm. Inertial sensors can also be used for motion tracking, I.E. regression of position in 3D space. Since the accelerometer measures acceleration in the sensor frame-of-reference, the linear acceleration can also be determined in the frame-of-reference of the room. The relative position change of the inertial sensor can then be calculated by integrating the acceleration signals, which will yield a displacement value in each sensor axis. This procedure of 'dead reckoning' can be used to infer the movement of the sensor but the noisy sensor data is very prone to an issue known as sensor drift [35]. Over long periods of time, the repeated integration of the relatively small noise values results in large error accumulation, necessitating more complex filtering algorithms such as Kalman filter [36] and sensor fusion approaches to reduce this drift error. This has been studied and demonstrated with Kalman filter algorithms by Mahony [37] and Madgwick [30], [38].

2.1.1.2 Vision systems

Vision systems typically monitor human activity using cameras that are placed throughout a room. Camera based motion capture systems use passive reflectors or devices that actively emit light to enable tracking in 3D space [39]. When placed on various limbs of the body they can be used to track the posture of the body in space. These systems require precise system setup but are highly accurate when calibrated.

Systems like the Kinect camera combine a visible spectrum camera with an IR three-dimensional depth sensor and can be used to enable human motion tracking without the use of optical markers [39].

The introduction of these technologies in a patient's home raises concerns about data security and unauthorized access to personal health information that is recorded or displayed in a private setting [15]. Additionally, such camera solutions require adequate distance from the participant for a complete field-of-view, so that the participant can be seen properly. This introduces space limitations, which can be difficult to achieve in a home setting [14],[40]. These systems are also restricted to a single room; this reduces the effectiveness of a vision system for human activity monitoring in a home environment.

2.1.1.2.1 Visible Light Positioning

Another particularly new area of research for vision-based sensing is visible light communication (VLC) and visible light positioning (VLP). Visible light communication (VLC) uses visible spectrum lights like LEDs to convey information. One such way to convey information is through modulating the light intensity at a high speed which cannot be perceived by the human eye. Specific known modulation schemes can be utilized to convey information at high speeds [41] and across large distances [42]. Visible light positioning (VLP) can relate the position between transmitters and receivers by measuring how the signal link changes with distance.

Visible light positioning is typically between fixed transmitters and a mobile receiver. The distance between different devices is determined similar to a GPS system, through the use of trilateration and triangulation. The distance from a light transmitter to a light receiver can be calculated using several different phenomena; this includes the time

difference, phase difference, or intensity difference of the signal. The signals can then be input into a position algorithm for determining the position in 3D space.

A typical VLP system might employ standard light hardware with modulators and then use a receiver to decode the received signal and incorporate a positioning algorithm to estimate position. Basic proof of this concept has been demonstrated with several various studies using light intensity difference against a fingerprint database [43] [44] of light intensity values, time difference of arrival (TDOA) [45], Received signal strength (RSS) [46], or hybrid methods using Angle of Arrival (AOA) and RSS techniques [47] for improved accuracy in 3D space.

While many of these systems would be suitable for motion tracking and activity recognition based on their accuracy values in the millimetre range, no commercially available solutions could be located. Additionally, many of the published systems for position utilize lab-grade and commercial hardware, which makes them cost prohibitive for many applications, such as home use. Some systems use signal generators ([43][44][48][49][47][50][51]) to modulate the transmitter, where estimated costs are $90,000 USD. The two studies that used affordable integrated circuits to modulate the transmitter signal were Vonkulbhisal [52] and Won et al [53], which used an LM324N operational amplifier and an M430F5438A microcontroller and obtained positioning error of 149 millimetres and 30 millimetres respectively.

An investigation into the feasibility of a visible light position system was undertaken in Lui et al [54] to determine the feasibility of building an affordable VLP system and to explore if alternate optical systems might be effective for human activity recognition. A visible light positioning system was built that measured 480 x 480 x 805 millimetres (Figure 2.2). 4 visible spectrum LEDs were placed above the positioning system and were

individually modulated at 1, 10, 40, and 100 kHz respectively with a commercially available LMC555 timer integrated circuit (IC) (Figure 2.3). The receiver (Figure 2.4) is a silicon PIN photodiode (OSRAM BPW34B) with a 60° half-power semi-angle, 7.45 mm^2 sensor area, sensitive to wavelengths from 350 to 1100 nm, peak sensitivity at 850nm, and spectral sensitivity of 0.2 A/W at 400nm. The photocurrent is converted into a voltage by the transimpedance amplifier, split into four channels by four suitable bandpass filters and then converted into DC voltage by RMS-to-DC converters. The receiver system is portably powered with dual supply +/- 9V DC batteries. The signal from the photodiode is amplified by an OPA380 precision transimpedance amplifier, bandpass filtered by a MAX274 configurable filter, and converted to DC value with AD736 IC. The resulting DC signal is converted from analog-to-digital (ADC) by a common ADC device, such as one that can be found on an Arduino Uno microcontroller.

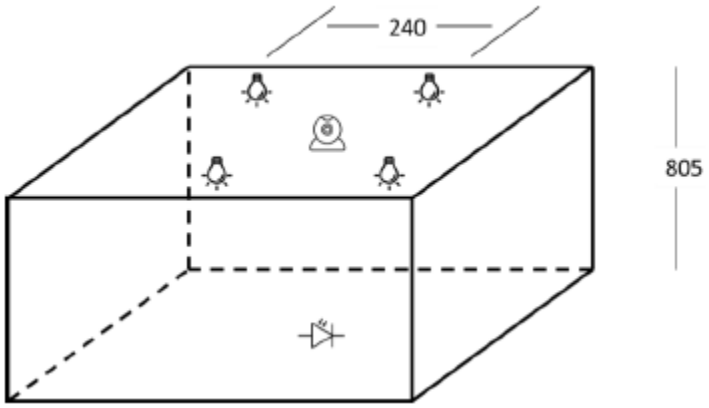

Figure 2.2. Visible Light Positioning System Diagram

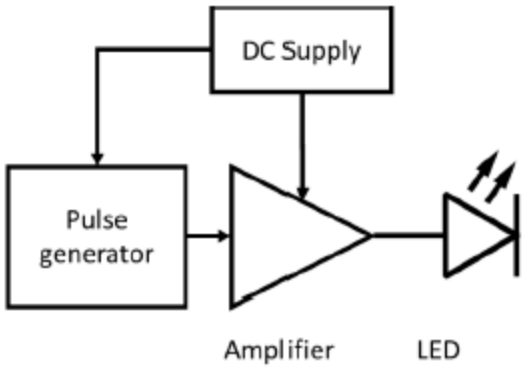

Figure 2.3. VLP Transmitter Block Diagram

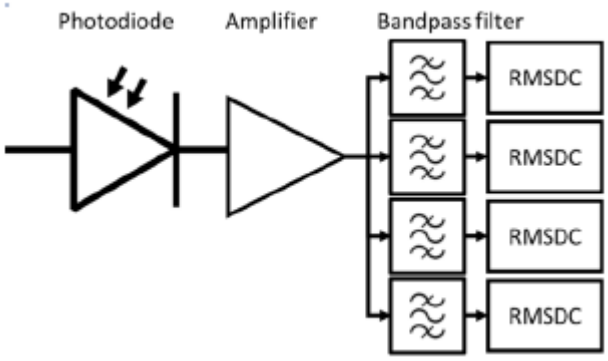

Figure 2.4. VLP Receiver block diagram

The positioning algorithm is performed by measuring signals throughout the bounds of the test system and building a single fingerprint database from the 4 transmitters. 2 dimensional Gaussian trends were fit to each signal channel to allow interpolation of signal values (Figure 2.5). For position determination, the signal data is compared to the fingerprint database. The position in the fingerprint database with the lowest sum of squared error was selected. Error values of 13.44 +/- 0.36 mm were obtained over 3 trials.

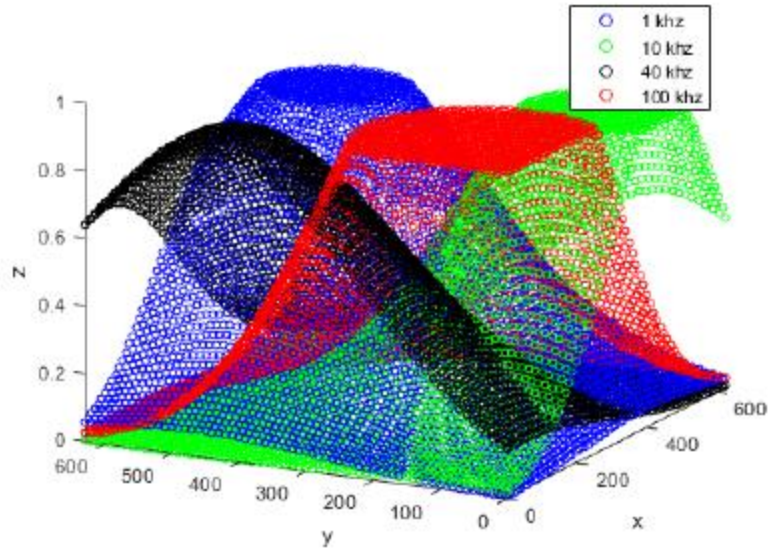

Figure 2.5. 3-dimensional visualization of signal strength

The results of this investigation indicated several findings. An economical system with individually modulated LEDs can be used for 2D positioning in a controlled environment. The system is low power and was proven to function portably.

Several limitations of fingerprint positioning VLP systems were also discovered. The system performance of fingerprint and RSS systems are limited to close distances. Beyond a critical distance, the signal-to-noise ration becomes critically low [55] and then reliable positioning is not possible. More advanced transmitter methods like TOA or TDOA would be necessary for farther distance positioning, however, these typically require transmitters to transmit in syncrony. One such method to accomplish transmitter syncronization is through the use of a single oscillator and individual frequency multipliers [45].

Additionally, RSS and fingerprint systems are susceptible to changes in their environment. Introducing new objects which block the transmission path between transmitter and receiver might otherwise change light transmission and reflection

properties of the environment, leading to error in these positioning systems. A summary of the advantages and disadvantages of a visible light positioning system for human activity recognition is compared to the more typical solution of using an inertial system.

The conclusion of the feasibility assessment for a VLP system for human activity recognition indicated that such a system was nearly realizable with existing hardware and capabilities, but had several significant drawbacks (Table 2.2). The author thus decided that an on-body sensing system was still ideal for the purposes of tracking a person's activity in multiple environments.

Table 2.2. Comparison of VLP and inertial technology for activity recognition

	VLP system	**Inertial System**
Advantages	• Objective position • High spatial precision/accuracy • Can be retrofit into existing room lights	• Portability • Proven technology • Commercial hardware available
Disadvantages	• Fixed to a single room • Size • Price • Optical occlusion • Performance drops as distance increases	• Relative motion • Complex algorithms (pose recognition or dead reckoning) and filtering required to extract movement information and reduce noise

		• Sensor noise and drift

2.1.1.2.2 Optical sensors (Thermal / Light)

Optical sensors generate an electrical charge in response to photons hitting the surface of the sensor. Each sensor material is sensitive to a different wavelength of light, which can range from ultraviolet (UV), visible light, infrared (IR), or beyond.

Studies have demonstrated the ability of a visible light sensor to identify landmark objects near the user such as lamps and windows [3]. Similarly, light sensors placed throughout the room can be used to sense the presence of a user, as mentioned in Patel et al [9].

Visible spectrum cameras for photography and video recording operate on this principle. Video based vision solutions to human activity tracking are discussed in the following section.

2.1.1.2.3 Thermal spectrum human activity tracking

Human motion can be detected using pyroelectric sensors which are sensitive to changes in heat flux that result from heat sources in the sensor FOV. Humans with a regular body temperature of 37 degrees Celsius will emit radiation around a peak wavelength of 9.4 micrometres based on the blackbody radiation curve and Planck's constant [56] [57]. The pyroelectric sensor material becomes electrically charged in response to a change in its temperature. Thermal radiation results in a temperature change, which alters the charge density of the sensor. This altered charge can be measured as an electrical signal, and requires amplification for useful interpretation. Note that transimpedance single amplification [58] is usually employed since the relationship

between current and thermal radiation is more linear than the relationship with voltage. Pyroelectric sensors have previously been mounted in living environments for sensing the presence of a person, [23] [21].

Note that thermal compensation is required for the sensors since any temperature changes (subject or environment) can cause a signal change from the sensor. Many devices use two elements in differential configuration to negate ambient temperature effects [56] or incorporate circuitry to process thermal signals on board and compensate for the ambient temperature of the environment [59]. The resulting output signal can be seen in Figure 2.6 below from the positive and inverted (negative) sensors of the differential detector. Devices with built in re-calibration or compensation for thermal effects are useful for the purposes of this investigation since this study is focused on system building and motion classification, not the low-level sensor design.

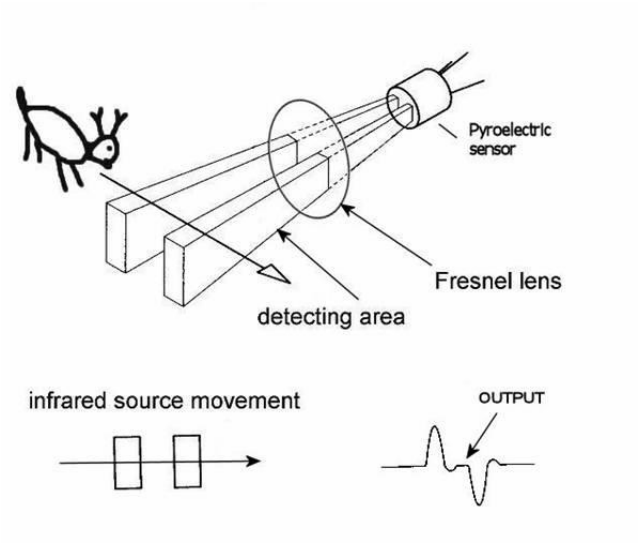

Figure 2.6. Differential pyroelectrical configuration from a manufacturer. [60]

Since infrared sensors would be specifically sensitive to heat sources in the environment such as humans, pets, electronics, and lights, this sensor information could be used in a controlled environment to determine the presence of a person in the sensor

FOV. If the sensor is mounted on the body, the relative orientation of the sensor could possibly be determined relative to the person. This could be useful for determining the orientation of a person's limb relative to their body during motion classification.

In the example image (Figure 2.7), a 4 by 4 passive infrared (PIR) thermal sensor is directed toward a person. The temperature reading in each sensor element is displayed as a brightness value in the image; higher temperatures are displayed as a brighter pixel while lower temperatures are represented by a darker pixel. As the person moves laterally through the sensor FOV, the signal in the image changes. Note that the darker pixels correspond to the room temperature, which is around 21 degrees Celsius. The brighter pixels are oriented toward the person, where the temperature is generally above 30 degrees Celsius. Several of the brighter pixels are seeing the person's body since their body and clothing are warmer than the surrounding environment. The brightest pixel near the top of each frame corresponds to the person's head; this temperature reading is higher because the exposed skin of the face is not occluded by clothing and thus results in a higher temperature than the rest of the person's body. This information could possibly provide some insight into the relative orientation between the sensor and person in FOV.

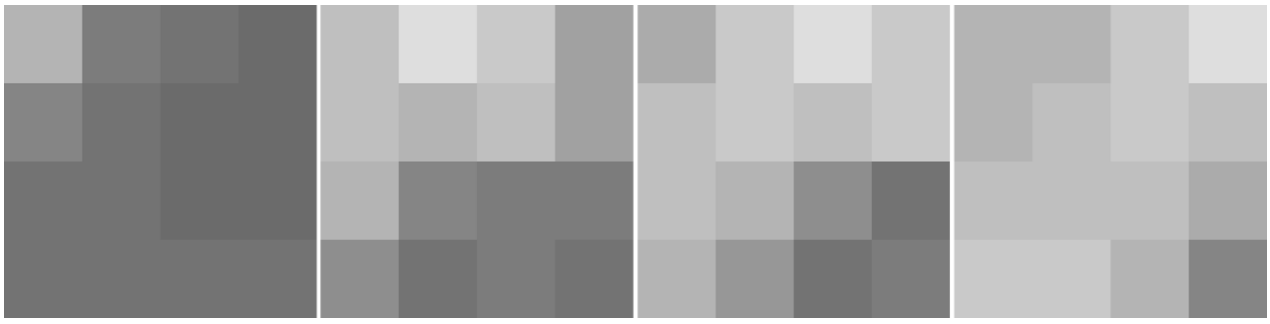

Figure 2.7. Change in thermal sensor values as a person moves through the FOV

2.1.2. Data pre-processing

Data pre-processing is helpful to separate the desired signal from noise sources that might corrupt and degrade the quality of classification performance [3]. Compensating, quantifying, or correcting for these values is important to improve detection accuracy.

Noise sources can include:

- Soft tissue movement, or external vibrations of a moving vehicle [61]
- Movement of the sensor on the wearer's body due to shifting of clothing
- Physical impairment such as tremor
- Electrical and magnetic objects near the sensor
- AC mains voltage
- Sensor heating can affect accelerometer and gyroscope values over time through thermal drift

Noisy high frequency signals can be removed with median filters according to Allen et al [62] and Mathie et al [61]. High-frequency electrical noise from nearby devices is commonly filtered with a median filter [63], average filter [64], or digital low pass filter (LPF) [65]. Yang et al [66] similarly advocate for a smoothing algorithm using a moving average, claiming that this removes jitter and noise from the signal.

Most of the gravity component signal is found in a low frequency (0.2 – 0.5 Hz) range; applying a low-pass filter can aid in separating body acceleration changes from gravity acceleration changes, according to Allen et al [62] and Mathie et al [61]. Foerster et al [67] also separated DC and AC signals with a 0.5 Hz LPF and applied a second 12 Hz LPF for the accelerometer. They found that separating the AC and DC components of

movement can provide useful insight into motions that occur at faster and slower speeds. In cases where the sensors are not fixed securely to the limbs and might be vibrating (during vigorous exercise), the filtering of DC and AC components separately might help reduce incorrect activity classification. Similarly, Zhou et al state that applying a LPF with a cut-off frequency of 10 Hz is sufficient for arm motion studies where most motions are much slower than 12 Hz [68].

In scenarios where activity classification is desired on a continuous basis, the segmentation of individual activities is required. It is important to consider differentiating the performance of various actions from one another; it also pertinent to consider differentiating action from inaction. Segmenting the continuously acquired data is a challenging task, and is often performed by: looking for characteristic periods of inactivity; segmenting activities based on energy levels; or comparison of relative sensor values from different devices [3].

A moving window is commonly employed in the case of continuous activity classification. The moving window allows complex or sustained activities to be detected, such as walking or sweeping. A moving window with a 50% overlap has demonstrated success in DeVaul et al [69] where activity states such as sitting, walking and biking were classified using accelerometer data and in Van Laerhoven at al [20], where sitting, standing, walking, running, stair climbing and biking were classified.

2.1.3. Feature extraction

Extracting meaningful features from raw and filtered sensor data is commonly performed in activity recognition systems to extract additional meaning from recorded sensor data [63] [69] [3]. The resulting features should ideally allow clear differentiation between different motions, leading to strong performance of the classification system. The

features selected should perform consistently; the features should reliably differentiate motions across different people and scenarios.

Mean

Mean acceleration features have demonstrated success in Bao et al [70] and Aminian et al [71] Median filter is also described in Foerster et al [67]. Both mean and median filters will somewhat reduce high frequency noise in data; however, the median filter will tend to better preserve the signal while more fully rejecting high frequency components. The mean filter will tend to smooth the data and incorporate the high frequency noise, causing more distortion to the underlying signal, but still reducing the presence of the noise in resulting data.

Standard deviation and variance

The variance of signals has been used to differentiate different ambulator motions such as sitting, walking, running, standing, biking, etc. The K means Cluster map in Yang et al [66] shows that the standard deviation of motions (y axis) varies more between classes than the mean signal (x axis) in each class. Similarly, Bao et al [70] indicate that the variance of a sensor channel can be used to capitalize on the different signal range for different motions.

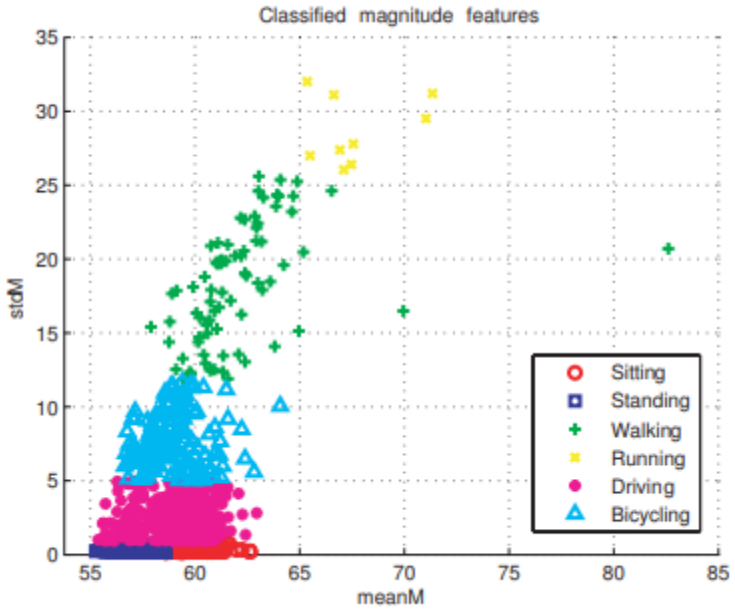

Figure 2.8. Differentiating motion classes using the standard deviation of a signal. [66]

The zero-crossing rate is described in Yang 2009 [66] as a useful time domain feature. It is possible that the zero-crossing rate may differentiate between repeated, oscillatory motions and unrepeated, linear motions (Figure 2.8). The zero crossing rate can be simply calculated as the number of times that a signal value crosses the x axis.

Frequency based features

Frequency domain features can provide a different insight into the motions recorded, especially for repetitive motions [3]. The energy of the accelerometer signal can be used to differentiate activities of varying intensity, such as sitting, walking, and running [70]. The energy of the signal was calculated by summing the squared discrete Fast Fourier Transform (FFT) signal magnitudes. The Discrete Fourier Transform (DFT) is given by:

$$X(f_k) = \sum_{n=0}^{N-1} x[n]\, \mathrm{e}^{-j2\pi f_k n} \quad (4)$$

For M frequency windows in the DFT signal, the energy value is calculated as follows:

$$Energy = \sum_{i=1}^{M}(DFT\_MAG(i))^2 \quad (5)$$

Signal Entropy is described in Yang 2009 [66] and Bao 2004 [70] as a possible method to differentiate motions that might have similar energy values, such as biking and running (Figure 2.9). The uniform motion of the legs in biking as opposed to the varied motion of legs during running may result in different distributions of frequencies of motion, and this would be differentiated more easily with entropy than with signal energy. The signal entropy can be calculated as the negative logarithm of the probability mass function.

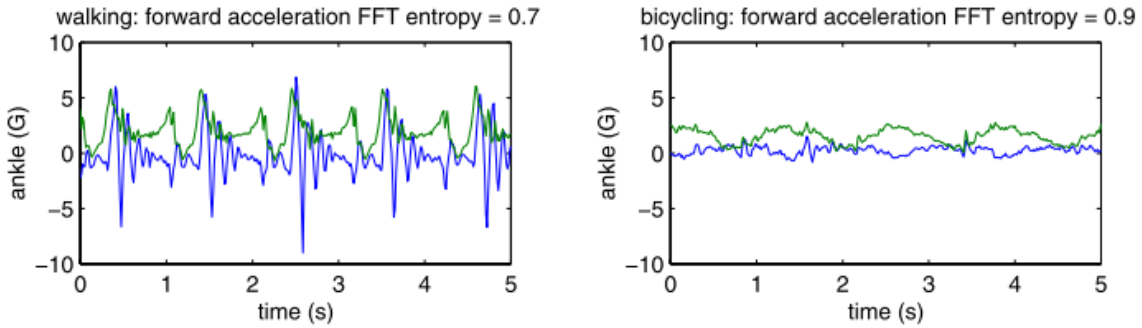

Figure 2.9. Entropy values in running and biking based on ankle accelerometer. [70]

Dominant frequency in the frequency spectrum can provide useful insight into the repetition speed of motion, such as the cyclical leg motions in running or cycling. The dominant frequency in the frequency spectrum is taken from FFT or power spectral density (PSD). Zhang 2016 obtained the dominant frequency at the peak value of the PSD [63] and Yang 2009 obtained a centroid of the power spectrum [66]. Additionally, the correlation between signal channels could be useful for differentiating movements involving multiple limbs [70], but this is not relevant in a study using a single device system.

Other considerations

DeVaul 2001 [69] found that the power spectrum of accelerometer magnitude might be a good feature to classify motion state. Yang 2009 [66] found that vertical features contain more information than horizontal features in an ambulation motion study. Yang 2009 [66] also found that time domain features are sufficient for most daily physical activity classification. This is an important consideration for real-time classification systems since time domain features have much lower computational complexity than frequency domain features.

2.1.4. Classification and Machine Learning

Many such types of machine learning models have been used for human activity classification. Some of these include the binary tree, k-nearest neighbours (k-NN), Linear classification, support vector machines (SVM), and Neural Networks (NN) [5].

2.1.4.1 Binary Tree

Binary decision trees have been used in multi-accelerometer systems for activity classification of up to 20 motions with accuracies ranging from 84-99.3% [5].

The feature space for decision trees are partitioned into subregions based on value thresholds for one or more of the feature space parameters (Figure 2.10). These resulting subregions can be further divided independently. These trees can be built manually or learned with an algorithm against a labelled training dataset.

When learning the tree nodes and thresholds with a learning algorithm, careful analysis and optimization are required since the calculation of all possible combinations is not computationally feasible. A greedy optimization algorithm is employed to choose the optimal subregion, the parameter, and the threshold value at a particular iteration. The

mechanism to stop model learning can occur after a threshold residual error is encountered; however, it is common to grow a larger tree to examine the possible error reductions, and then remove tree nodes (prune back the model) to yield a simpler and more sensible tree structure that still delivers an acceptable prediction performance. This optimal tree size can be quantitatively found by cross-validating the dataset and can help reduce the overfitting of the model to the input training data.

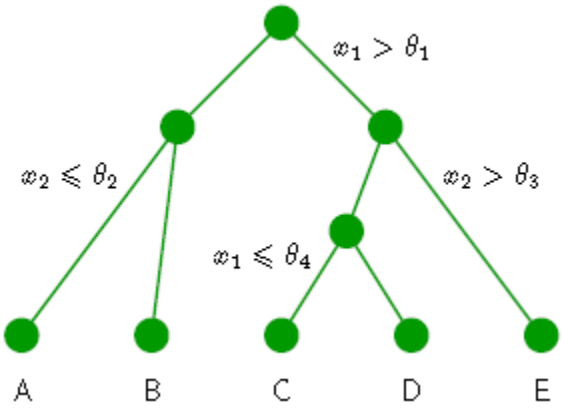

Figure 2.10. Binary Decision Tree structure. [72]

2.1.4.2 Nearest Neighbors

The k-Nearest neighbor classification has been used in activity classification in studies up to 20 activities and with accuracies up to 86.6% [5]. K-nearest neighbors is a non-parametric classification approach. The k-NN approach can be a useful alternative to kernel-based approaches which may perform poorly on datasets where the density of data varies widely across the input space, [72]. Relying instead on a finite number of neighbours around a given point can help to control this issue.

Note that changing the neighborhood size K will affect the smoothness of the resulting decision boundaries and even the classification result. In Figure 2.11 parts A and part B, the classification result is affected by the number of neighbours that are examined

in the local neighbourhood. In the k-NN examples in part C and part D, the prediction class does not change when k changes from 5 to 11. A small K will select the single closest neighbor and result in sharper decision boundaries (Figure 2.12). A larger K value will result in fewer, smoother decision boundaries.

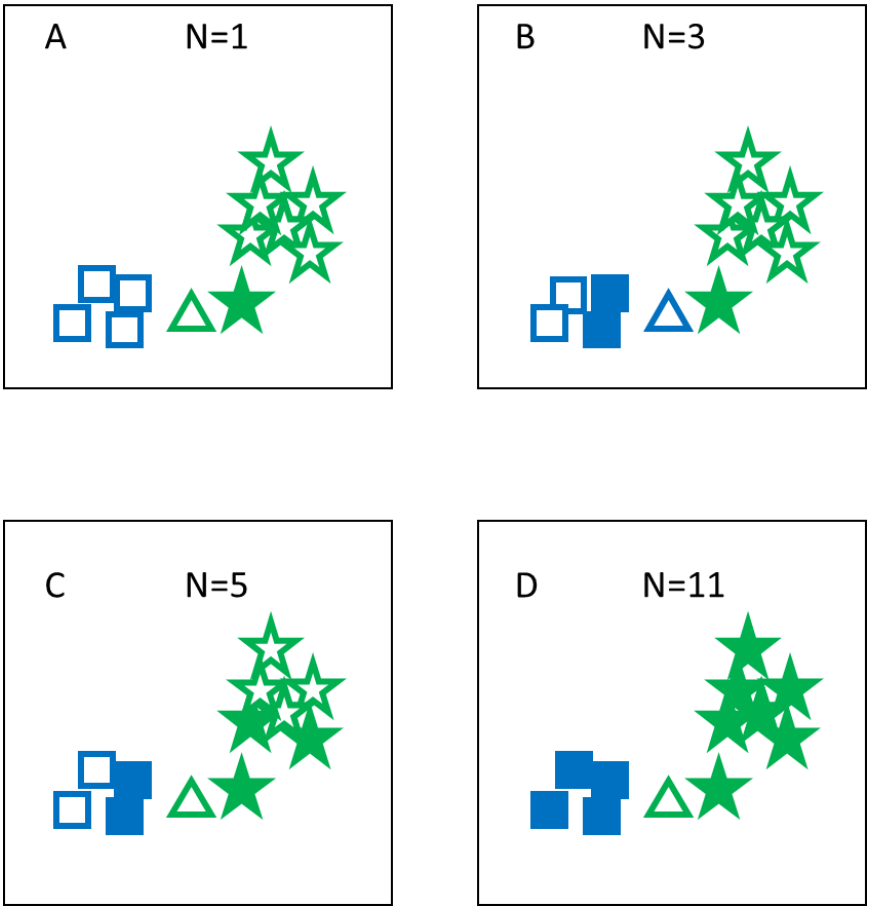

Figure 2.11. Effect of Neighbourhood Size on K Nearest Neighbours

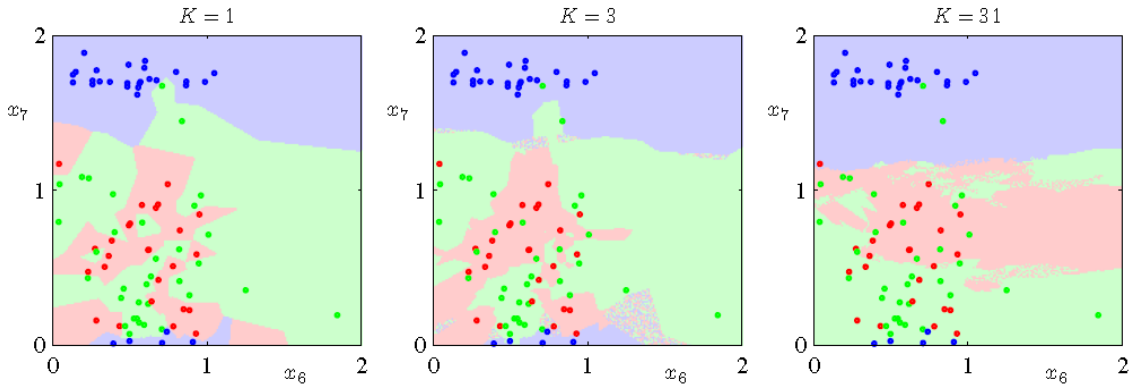

Figure 2.12. Decision boundary smoothness is affected by neighborhood K value. [72]

One disadvantage of the k-NN model is that the entire training dataset should be stored, possibly leading to expensive computation for large datasets. However, some efforts can be taken to reduce the need for exhaustive searches through the dataset; an example would be representing data in a search structure such as a tree.

2.1.4.3 Linear classification

Linear discriminant analysis (LDA) determines discrete class membership using linear combinations of the features in the input data vector. The class membership prediction is output from a discriminant function, which is a form of the activation function.

A simple representation of a two-class problem with two input dimensions, x_1, x_2 is described in Figure 2.13. The linear discriminant is the line that best separates the two classes. While the data might not be easily separated in the x1 or x2 axis, the data can be easily separated using a line in the 2D x1-x2 feature space.

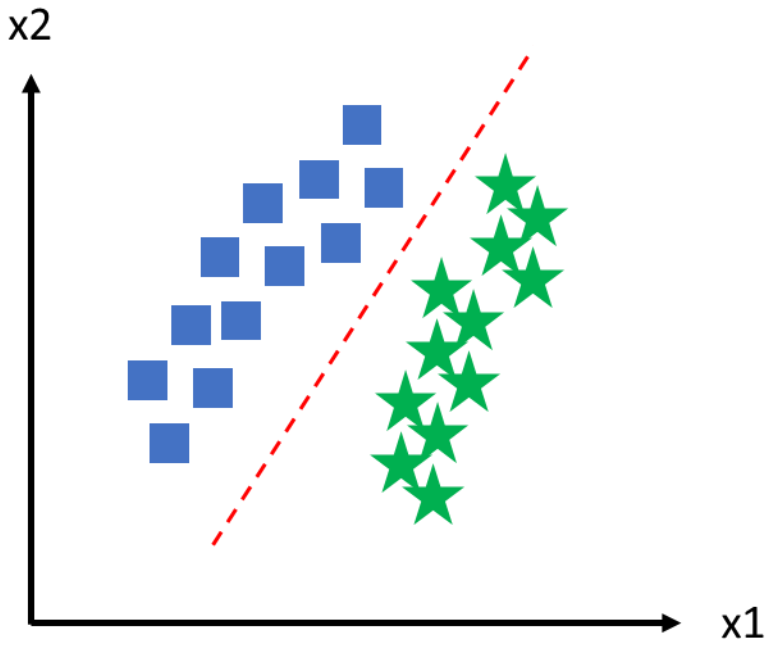

Figure 2.13. Linear discriminant as a function of two input dimensions. [72]

For multiple classes, the one-vs rest classifier is used to perform K-1 classifications for the K classes. Note that this can result in ambiguous prediction space. In a case where 3 different classes are classified with 2 different linear discriminant functions, an ambiguous decision space can be created (Figure 2.14).

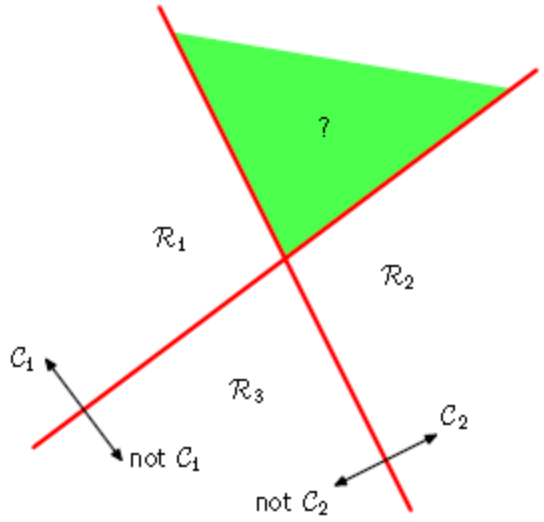

Figure 2.14. Ambiguous prediction space using K-1 one-vs-rest classifier method. [72]

Alternatively, the one-versus-one classifier can be used. This uses K(K-1)/2 binary discriminant functions for each pair of classes. The class prediction can then be determined as the majority vote from the classifiers. Note that ambiguous decision spaces can still result from this method (Figure 2.15).

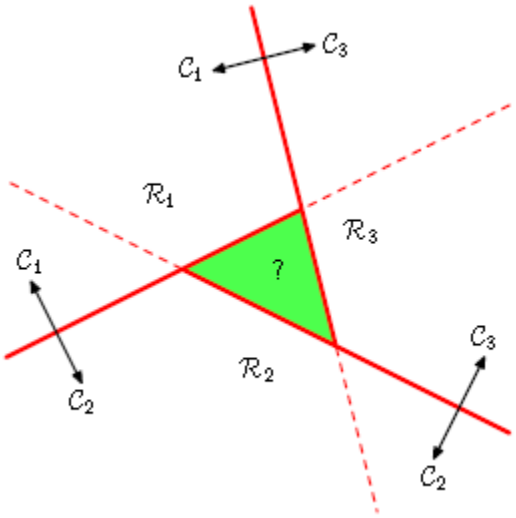

Figure 2.15. Ambiguous decision space in a one-versus-one classifier. [72]

A solution to the ambiguous problem spaces can be obtained by using a K class discriminant (Figure 2.16). By design, the problem space appears as a D-1 dimensional hyperplane. The decision regions are all convex.

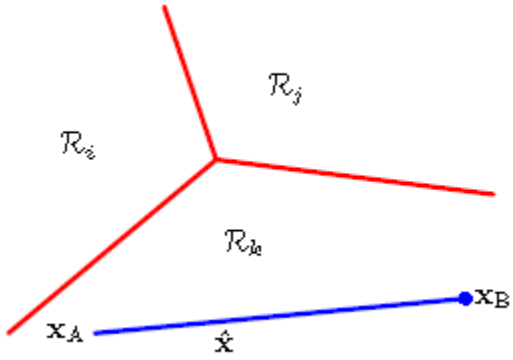

Figure 2.16. K class linear discriminant analysis. [72]

2.1.4.4 Support Vector Machines

Some learning algorithms are limited because the kernel function is evaluated at all possible binary pairs of training points, which results in unrealistic computation times. Sparse kernel-based algorithms are desired, which depend only on kernel function on a subset of training data.

SVM model parameters correspond to a convex optimization problem, which makes for a more stable solution finding process. With a convex optimization problem, a local solution is also the global optimum.

SVM is similar to linear classification since a linear combination of input parameters is used to define a line or plane through points to separate different classes. In the linear classifier between two classes, this was modeled as $y(x) = w^T\phi(x) + b$. However, in SVM, only a subset of the training points is used to obtain the parameters of

the separating line or plane. The subset of points examined to determine parameters of the decision boundary are called support vectors.

The SVM aims to minimize the generalization error of the model by maximizing the margin between the decision boundary and the closest sample data (Figure 2.17). This margin is the perpendicular distance between the decision boundary and the closest sample. Visual of decision boundary and the margin is shown below. The support vectors are denoted as circles, and the margin is the distance from the red decision boundary to the closest samples.

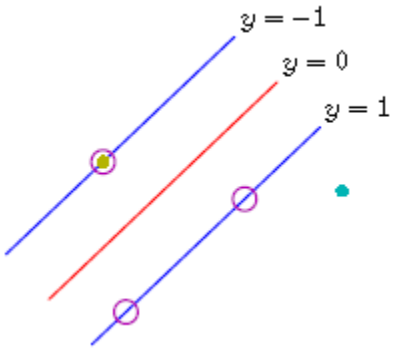

Figure 2.17. SVM Classifier Margin. [72]

Input data to the SVM model is transformed into the kernel function's space so that a linear relationship can be found between input and output values. A commonly used kernel function is a Gaussian kernel. The advantage of the nonlinear kernel, like the Gaussian kernel, is that while a data set might not be linearly separable in a 2D input space for x, the data is linearly separable in the nonlinear kernel feature space, [72]. The contour lines in a Gaussian kernel (Figure 2.18) indicate areas of constant classifier function value y(x), and the support vectors are denoted with circles.

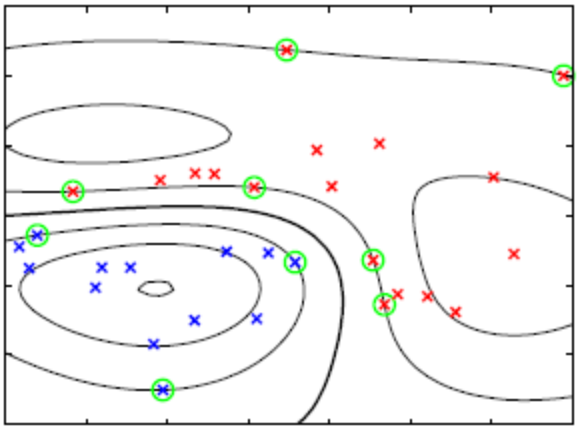

Figure 2.18. SVM solution using Gaussian kernel. [72]

Note that the SVM model does not output probabilistic outputs. Closely related Relevance Vector Machines (RVM) should be used if probabilistic outputs are required [72]. Also, note that SVM models often require empirical parameter optimization during model fitting [73], which can be problematic when datasets might be small or not fully representative of all future data input.

2.1.4.5 Neural Networks

Neural networks can improve on some limitations present in support vector machines. The multilayer perceptron is one example of a neural network. The model can be evaluated more quickly than an SVM model.

A neural network is a set of linear activations, known as neurons, which relate the inputs and outputs of a system through one or more series of hidden layers. The outputs from the network can be used to yield a finite classification prediction or a continuous valued output.

A singular neuron in a network consists of an input, an activation function, and an output value from that neuron. A neural network consists of many connected neurons. The neurons are arranged in layers such that the output of several neurons will serve as inputs

to subsequent neurons (Figure 2.19). The strength of a relationship between a neuron's output and another neuron's input is reflected by a relative weight value. These neuron structures and activations are inspired by the structures and interlinking relationships of biological neurons in the human brain.

In the figure below, the first column of neuron nodes is the input layer, the last column is the output layer, and the middle column is the hidden layer of the neural network. X denotes input neurons, z for hidden neurons, and y output neurons. The weight relationships between each neuron are denoted by w.

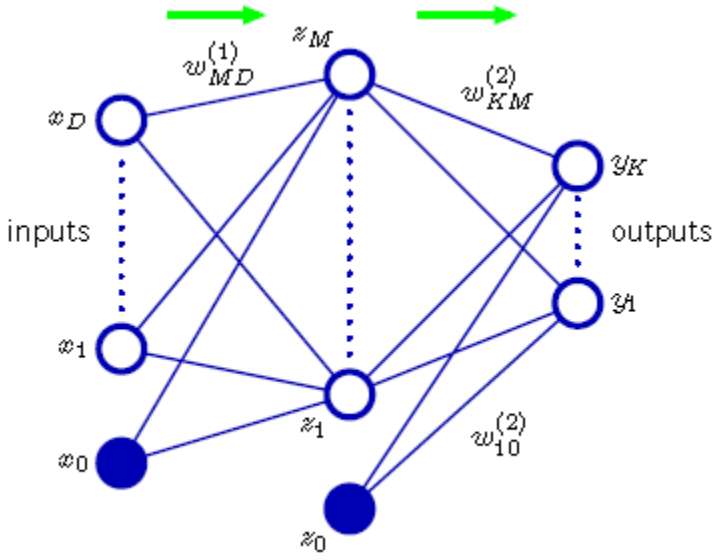

Figure 2.19. An Example of a Neural Network. [72]

For D input variables $x_1, \ldots, x_D$, combinations are constructed between each of the D input variables. For a neural network with M neurons in each hidden layer, a fully connected neural network will have D x M neuron connections at the first layer. The activation of an individual neuron in the first layer, a_j, is given by each of its D connections to the D different input variables. For each of the M neurons in the first hidden layer $a_1, a_2, \ldots, a_j, \ldots, a_{M-1}, a_M$, the activation of a neuron is determined in the forward

propagation calculation based on the weights w_{ji} and input variables x_i. Each weight w_{ji} describes a learned weight value between an input x_i and a hidden layer neuron, a_j.

$$a_j = \sum_{i=1}^{D} w_{ji}^{1} x_i + w_{j0}^{1} \quad (6)$$

The individual activation functions are usually nonlinear functions such as the logistic sigmoid or tanh function [72]. The linear combinations of these nonlinear functions are then used to process training data and find the optimal set of weights, w, which minimize classification error.

In the case of multiple class classification, an output neuron will be present for each possible output class. Each output class activation function is usually a logistic sigmoid function. In a mutually exclusive multiclass classification, a softmax activation is usually employed at the final stage of the classifier [72]. While probability estimates of each class sum to 1, the predicted class is usually selected as the single highest probability in the softmax output vector.

$$\sigma(a) = \frac{1}{1+\exp(-a)} \quad (7)$$

2.2. Related Work

A summary of related work in activity classification is summarized here.

2.2.1. Wearable systems: Multi Device Inertial systems

Wearable sensor systems consist of single or multiple devices that are worn by a patient, and the movement of the patient is measured directly from their body. Unlike vision systems, wearable sensor systems do not rely on a visualization of the patient and their personal home.

Wearable sensor systems frequently use accelerometer or gyroscope sensors, or combined units called inertial measurement units (IMU). Systems with multiple separate devices are frequently proposed for sensing the orientation of each limb, allowing the position of each limb to be obtained by solving the relevant kinematics equations.

Wearable sensor systems can consist of single or multiple devices with each device serving a specific purpose. For example, a multi-device of this system might require separate devices for sensing movement and orientation of each limb, which is then used to determine the position of each limb by solving kinematic equations.

An example of a wearable sensor system is the Xsens MVN Motion capture suit which has 17 sensors to track multiple limbs on the body [74] (Figure 2.20).

Figure 2.20. Xsens MVN IMU Suit for motion capture. [74]

Some studies have reported considerable classification accuracy using inertial sensors. Bao et al [70] reported 84% classification accuracy on user annotated data of 20 motions with 5 devices placed on the arms, legs, and waist. These motions included walking, sitting, running, brushing teeth, eating, and biking. Zinnen et al [75] reported 93%

classification accuracy for 20 motions with a 5 -device system, and 86% accuracy when 2 wrist devices are used. The motions in this study included opening and closing various doors of a car and a writing task. Zhang et al [76] proposed a 2-device system that classified 6 arm motions with 97.2% accuracy where the sensors were worn on forearm and bicep.

In wearable sensor systems, it is trivial that further addition of sensors would result in high accuracy; however, asking a patient to wear 17 or even 5 devices for each rehabilitation session is tedious and may demotivate the patient. Additionally, a multi-device system is more complex to don than a single device system, especially when units are placed on multiple limbs or a calibration between devices is required.

2.2.2. Wearable systems: Single Device Inertial systems

Single device inertial sensor systems implement algorithms to allow recognition of limb pose and their models can also be informed by the kinematic constraints of typical human motion. However, since the orientation of only one limb is known, the kinematic system is under-defined, and the pose of the limb cannot be determined through a forward kinematics solution [77]. A single sensor system is an underdefined system, which has had limited success in determining limb positions; however, the system has been shown to efficiently classify the type of motion being performed.

Several single-device systems have been proposed which track ambulation (running and walking) and poses (standing and sitting). Zhang et al [78] reported 96.1% accuracy for 9 activities that included walking, running, sitting, and standing with healthy participants. In another study, Khan et al [79] reported 97.9% accuracy on 15 motions with a chest-based device for various activities such as lying, sitting, standing, and transitions

between these activities. Ravi et al [80] classified 8 ambulation motions with 99.8% accuracy using a single device situated at the pelvis.

Placing a single-device wearable on the waist is considered an acceptable sensor location for tracking ambulation motion [6] and is recognized to cause minimal discomfort to the user. However, a waist-worn wearable is unable to track arm motions [6]. Falck et al [7] found that wrist-worn wearable devices have distinct advantages for activity monitoring. Some wrist-worn wearables are sufficiently comfortable for long-term use. This can reduce data loss by improving the compliance of the wearer.

Some single-device systems have been proposed for the classification of arm motions for healthy and stroke survivor populations. Tseng et al [81] reported a single device system with 93.3 % accuracy for classifying 3 motions related to opening a door in a study with 5 healthy participants. Panwar et al [82] conducted studies of motion classification for 3 drinking motions with 4 healthy participants and reported 99.8% accuracy when using a convolutional neural network (CNN). Biswas et al [83] reported 91-99% accuracy for 3 reaching arm motions with 4 healthy participants and 70-85% accuracy with stroke survivors. Yang et al [84] achieved 95% classification accuracy of 8 activities using a neural network; 4 of those actions involved some arm motion, while 4 other motions were primarily ambulation activities. Zhang et al [63] proposed a single IMU system for classification of 6 arm motions with 14 stroke participants and reported up to 99.4% and 98.8% accuracy with a novel model and a Support Vector Machine (SVM) model respectively. These 6 motions represented 4 of 7 degrees of freedom of the human arm: shoulder extension/flexion, shoulder adduction/abduction, forearm pronation/supination, and elbow extension/flexion. Movements representing shoulder abduction, wrist flexion/extension, and wrist adduction/abduction were not represented.

In summary, the author's literature review indicated the highest number of arm motions classified in a single-device system was 6 arm motions.

2.2.3. Infrared Sensor Systems

Bulling et al [3] suggested that light sensors might provide orientation information between a fixed light source in a room and the sensor frame of reference, which is typically fixed to a limb on the user's body. While these studies suggested a visible light sensor for the detection of windows and lamps in the room, it is possible that other optical sensors could offer similar benefits. Pyroelectric sensors are sensitive to thermal emissions from warm objects and should be able to robustly indicate when the warm object is in the sensor's FOV. Previous studies ([19] [20] [21] [22] [23]) have demonstrated feasibility for a pyroelectric sensor to determine the position of a user in a room or to aid a device in classifying ambulatory activity.

A review of studies that have explored optical sensors yielded the following contributions related to human activity recognition using visible and optical sensors. Several studies mount thermal sensors in fixed locations for sensing user position in a room. Fan [21] used an 8x8 element thermal sensor grid which was mounted in a room to detect the presence of a person in different regions of a living environment. Similarly, Akhlaghinia [22] used PIR sensors for room occupancy detection but does not use the sensor for motion classification. Bauer et al [85] used an infrared proximity sensor to detect when a user was close to an object of interest; this improved sensitivity of their activity classifier by signaling scenarios where the user might possibly use that object.

Some select studies have proposed systems for motion classification that incorporate thermal sensors. Hevesi [23] used a thermal sensor mounted in the room to detect the presence of a user in different areas of the household and detected usage of

various household cooking appliances based on the location of user activity. Lee et al [86] used a waist-mounted device to detect whether a user was walking on level ground, up an inclined or down a declining slope, although it was unclear how the incorporation of infrared light sensor aided the classification accuracy of the system.

Maurer et al [19] used a device fitted with an accelerometer, a light sensor, a temperature sensor, and a microphone to classify 6 different ambulatory activities (sitting, standing, walking, walking up stairs, walking down stairs, and running). Recognition accuracy was considerably high for most of the 4 motions but ascending and descending stairs accuracies were significantly lower, possibly implying that these two motions were quite difficult to distinguish from each other. Maurer noted classification accuracies for single devices were as high as 87% for a wrist mounted device, 90% when worn in a shirt pocket, and 93% when carried in a bag on the person. Maurer indicated that the performance of the light sensor for classification was the poorest of all sensors, with the wrist-based sensor classifying motions correctly 55% of the time. However, Maurer notably found that a select group of 8 features which included a root mean square (RMS) value from the light sensor value yielded comparable results to the full feature set. More motion types could possibly be classified based on the results; however, the performance of the system in respect to the number of motions classified was not challenged. It is unclear how well the system would function with higher numbers of motions, or with classifying arm motions.

Van Laerhoven and Cakimacki [20] used a large variety of sensors instrumented into a pair of pants, which included accelerometers, passive infrared (PIR) sensors, carbon monoxide sensor, microphone, pressure, temperature, touch, and light sensors. Varying accuracies of 45-96% were encountered with the resulting learning model but the relative performance contributions by each sensor were not explored.

Studies incorporating pyroelectric sensors for human movement detection have been demonstrated in studies such as Yun et al [87], which used a pyroelectric sensor to detect the presence of a person, their walking speed, and whether a person was walking close or far from the wall. Walking direction accuracy was around 99% while 3-speed classification accuracy was around 95%. Shankar et al [56] designed a system to track human position at distances of up to 12 meters using pyroelectric sensors with Fresnel lenses. This work was further elaborated in Hao et al [88], where pyroelectric sensors were distributed about the room and were inputted into Hidden Markov Model (HMM) and Kalman filter models to estimate user position within a room. Fang et al also furthered this team's work and explored the usage of pyroelectric sensors for a user identification system and identified users with individually trained HMMs with an average accuracy of 78.5%. Yang et al [89] deployed a mesh network of pyroelectric sensors spaced 5 meters apart and reported 0.5 meter accuracy in determining the position of a person. Note that the above studies focused on the tracking position of a single person within a room.

The literature review did not discover studies where thermal sensors or pyroelectric sensors were used for the classification of a user's arm motions.

2.3. Chapter Conclusion

A summary of current technologies and techniques for motion classification was explored, including a detailed discussion on some sensor technologies available for human activity recognition, techniques for data pre-processing and noise reduction, algorithms for feature extraction, and machine learning models for classifying human motion.

Inertial sensors will likely continue to play a significant role in on-body sensing systems due to its ability to sense the tilt angles and orientation of human limbs. The

addition of a thermal sensor is proposed for its potential to provide a valuable alternate source of data: the thermal signature of objects in its field of view. Also, an investigation into an alternate system for room-based motion tracking was explored; this method was ultimately determined to not be optimal for this study's objectives of improving arm motion classification. Sensor preprocessing will primarily employ a moving window average filter to smooth high frequency noise sources in the data. Feature extraction was discussed and will incorporate time-based features, such as mean and standard deviation, as well as frequency-based statistics, such as PSD peak characteristics and signal energy, to aid differentiation and improve the performance of the motion classifier. Finally, the motion classifier machine learning models and architectures were discussed.

Chapter 3.

System Design

This chapter describes the system design of the arm motion classifier, in support of Objective 1. The chapter is outlined as follows. Sensor hardware selection is discussed in section 3.1. Hardware and software design are described in sections 3.2 and 3.3 respectively.

Some preliminary work to explore the relative performance of each sensor was performed to guide the selection of useful sensors and is briefly summarized in section 3.2, with supporting figures placed in Appendix B.

3.1. Sensor Hardware Selection

A preliminary investigation was performed into arm position classification using a wearable platform that contained an inertial sensor in addition to pyroelectric and infrared distance sensors in Lui et al [90]. The findings from this investigation aided in sensor hardware selection. Due to the preliminary nature of this work, the relevant figures and tables are available in Appendix B.

The layout of sensors on the device is described below (Figure 3.1). Two 16-element Passive Infrared (PIR) sensors were mounted proximally on the wrist, with one sensor pointing upwards (“Omron 16”) and one pointing downwards (“Omron 16-2”). Two 8-element PIR sensors were mounted distally and were also individually oriented upwards and downwards. Additionally, four infrared distance sensors were mounted near the middle of the device and were staggered to point upwards and downwards. The device

was mounted on a foam pad and affixed to the wearer's wrist with Velcro straps (Figure 3.2).

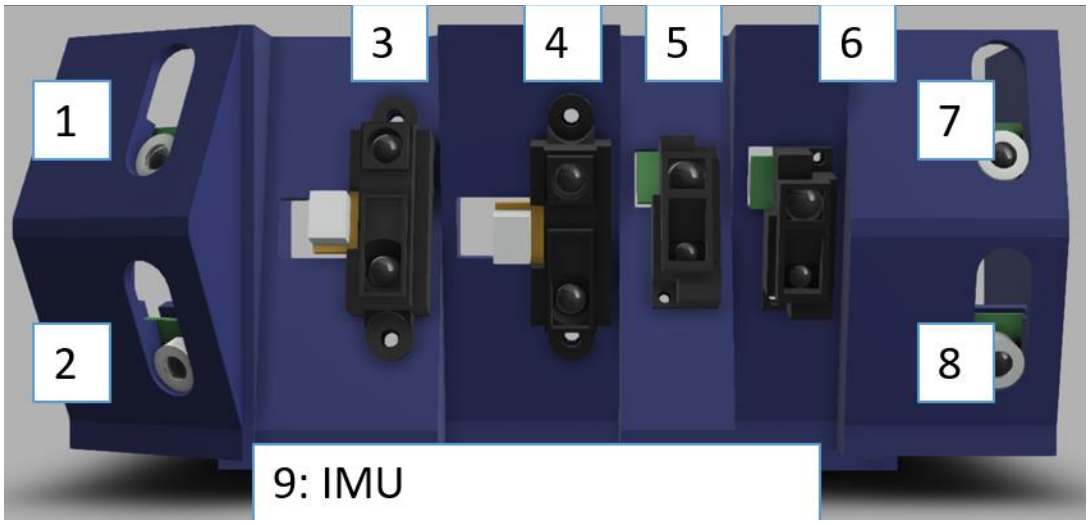

Figure 3.1. Rendering of the device used in the 2017 study [90]**. Labels [1,2]: 16 element PIR, [3-6]: IR Distance, [7,8] 8-element PIR**

Figure 3.2. The device used in the 2017 study [90]**, present with foam pad and Velcro straps**

A preliminary study in static pose classification was conducted with 5 healthy participants who wore the device on their left wrist. The participants moved their hands to 22 static poses while seated at a table. The raw sensor data was segmented into training and testing data and evaluated with a Linear Discriminant Analysis (LDA) classifier.

The study indicated that the proximal downward oriented PIR thermal sensor delivered a higher classification accuracy than other sensors for static arm poses. In the interest of miniaturizing the design and including only the required sensors, it was decided to remove the distal thermal sensors and the IR distance sensors, which provide relatively low performance contributions.

Further investigation will be required to determine how the thermal sensor contributes to motion classification. For the purpose of comparing the classification performance to existing work, the accelerometer and gyroscope sensors are retained.

3.2. Hardware

The proposed system is a single unit device (Figure 3.3) with the MPU9250 IMU [91] and the Omron D6T [92] thermal sensor. The device is situated on a custom-designed PCB and is controlled by an ATMEL CPU processor. The device's microcontroller was loaded with an Arduino Pro Mini firmware. A data acquisition program was then deployed to the device to read sensor data and then transmit via Bluetooth connection to a computer where the signal was recorded to disk. This code can be found in Appendix B. This data was received at 12Hz on a receiving computer.

The device is battery-powered and continuously acquires sensor data when powered. When the device is powered by a 1200 milli Amp-hour lithium polymer battery, the battery life is about 15 hours. When a recording device like a laptop computer is connected via Bluetooth connection, sensor data is regularly transmitted at a 12 Hz frequency. Sensor data interpretation and motion classification are performed on the computer. It is mounted on a soft foam band with straps, allowing it to be comfortably attached to the body (Figure 3.4).

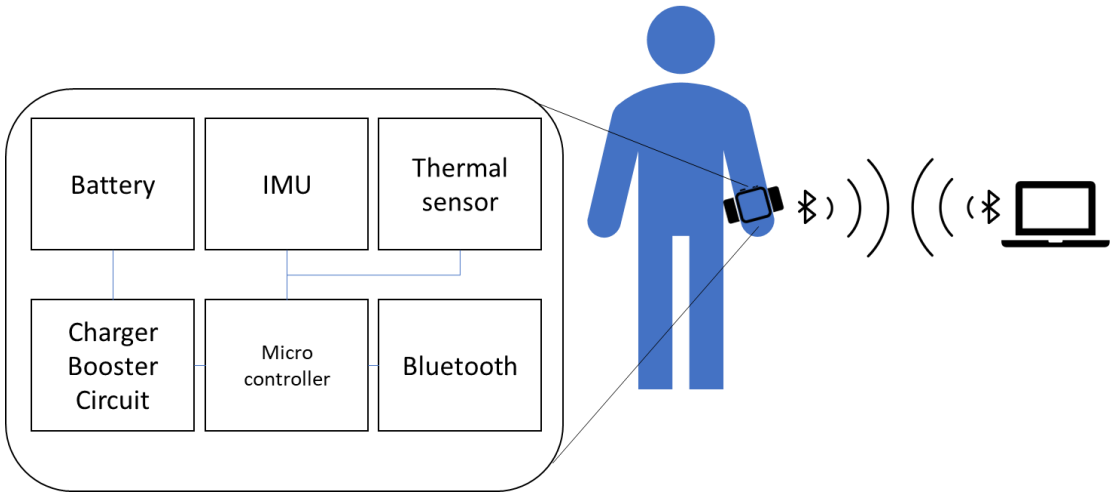

Figure 3.3. Block diagram of the proposed system

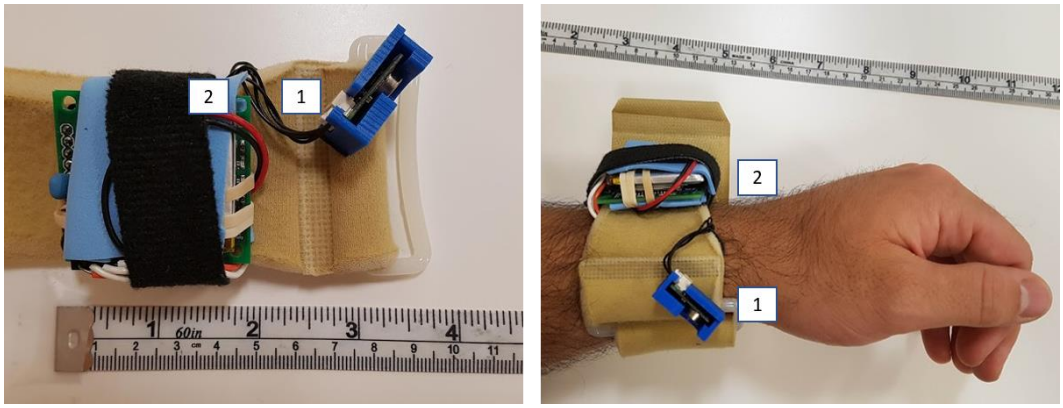

Figure 3.4. Images of the Device. (a) The device on a table, showing the thermal sensor (1) and the main unit (2). (b) The device positioned on the wrist.

The device has two main sensors: The MPU9250 IMU and Omron D6T passive thermal sensor. The MPU9250 [91] is an IMU with a 3-axis accelerometer, a 3-axis gyroscope, and a 3-axis magnetometer. The sensor data was transmitted to a recording computer at a 12 Hz frequency; similar studies have reported that signal data frequency of 10 Hz is sufficient to detect arm motions [68]. The Omron D6T [93] is a passive infrared thermal sensor that reports a 4-by-4 grid of temperature readings in its 45-degree by 45-degree Field of View (FOV) and can greatly aid in detecting the presence of a human

body, even through thick clothing. When mounted on the arm, the thermal sensor provides temperature data that can provide insight into the relative orientation between the user's wrist and body.

3.3. Chapter Conclusion

The proposed design is a single-device system which incorporates a PIR thermal sensor in additional to an inertial sensor. The device is mounted on a soft strap for comfort and can regularly transmit data to a receiving computer for several hours. The infrared sensor is mounted at a distal position on the device, pointing inward toward the user, as optimized in Lui et al [90]. Findings in this study indicated that the PIR thermal sensor has a better ability to predict static pose than an IR distance sensor or accelerometer. This system design for a single-device wearable that incorporates an IMU sensor in addition to an infrared thermal sensor satisfies Objective 1.

Chapter 4.

Methods

This section describes the proposed data processing and motion classification scheme in support of the system design (Objective 1) and describes the experimental methods for validating system performance in support of Objective 2. This chapter includes a description of the participants in section 4.1, experimental protocol in section 4.2, and finally a discussion on data processing and feature extraction in section 4.3.

4.1. Participants

11 healthy participants (6 female, 5 male) were included in this study. Their median age was 28 ± 6 years. All were right-handed. All signed a consent form for this study that was approved by the Simon Fraser University Research Ethics Board.

4.2. Experimental Protocol

The experimental protocol is described below. The device was worn on the left wrist with the thermal sensor located on the radial aspect of the wrist. When the forearm is neutrally oriented (arm posed so that the thumb is pointing upwards), the thermal sensor is oriented at a 45-degree angle from the radius bone such that it is pointing inwards towards the user's torso, Figure 3.4. Sensor orientation was configured to ensure that the user's torso is in the sensor FOV for most arm motions within a typical user's range of motion. The device is worn proximal to the radiocarpal joint to remove the unwanted influence of the wrist flexion actions. The device was worn on the left wrist for all participants in this study to maintain consistency of results. It is expected that similar results would be obtained if the study was conducted while the device was worn on the

right wrist. Lee et al [94] indicated that wearing inertial sensors on either wrist might be valuable in reviewing the physical activity of stroke survivors in a clinical setting.

4.2.1. Motions

Each participant was seated at a table and performed 24 motions with their left hand; these motions are described in Table 4.1. The motions were derived or adapted from rehabilitation protocols which are currently used for unilateral upper extremity rehabilitation: Chedoke-McMaster Assessment [16], CAHAI, [17], GRASP, [95], and Bobath [63].

Table 4.1. 24 protocol motions

#	Motion	Reference	Exercise notes
1	Bobath Handshake	[63]	Grasp hands together and raise arms upwards
2	Straight Arm Press	[63]	Place the palm on the chair and straighten the arm
3	Horizontal Shoulder Extension	[63]	Start with hand on the opposite shoulder and rotate shoulder outwards 180 degrees
4	Elbow to Nose	[63]	With the hand on the opposite shoulder, flex shoulder to bring elbow up to the nose
5	Touch Shoulder	[63]	From table to place hand on the opposite shoulder
6	Supinate	[63]	Arm on table, supinate 180 degrees
7	Pronate	[16]	Arm on table, pronate 180 degrees
8	abductShoulder90	[16], [95]	Arm at side, abduct 90 degrees
9	Reach 0 to 1	[95]	From centre position to marker “1”
10	Reach 1 to 0	[95]	Return from marker “1” to centre
11	Reach 0 to 2	[95]	From centre position to marker “2”
12	Reach 2 to 0	[95]	Return from marker “2” to centre
13	Reach 0 to 3	[95]	From centre position to marker “3”
14	Reach 3 to 0	[95]	Return from marker “3” to centre
15	Reach 0 to 4	[95]	From centre position to marker “4”
16	Reach 4 to 0	[95]	Return from marker “4” to centre
17	Reach 0 to 5	[95]	From centre position to marker “5”

18	Reach 5 to 0	[95]	Return from marker “5” to centre
19	Shoulder Flex 180	[16]	Arm at the side, flex shoulder 180 degrees
20	Hand to Forehead	[16]	The arm on the table, reach up to place hand by the forehead
21	Elbow Flex 90	[16], [95]	The arm at the side, flex elbow 90 degrees
22	Pick up Phone	[17]	The arm on the table, pick up the phone
23	Zip Upwards	[17]	Zip upwards from waist to neck
24	Zip Downwards	[17]	Zip downwards from neck to waist

4.2.2. Workspace

Participants completed the protocol while seated in a hard-backed chair with no arm rests in front of a table in a research laboratory (Figure 4.1). Motions 1-8 and 19-24 were completed with the participant sitting with their back against the chair, and the arm positioned at the appropriate starting position for each motion. The 10 grasping motions (9-18) were completed with 5 markers that were spaced radially from a central marker on the table as per the GRASP table-top reaching protocol [96], and a soft foam ball was held during these tasks. The outer circles were placed at a 35 cm distance from the central point.

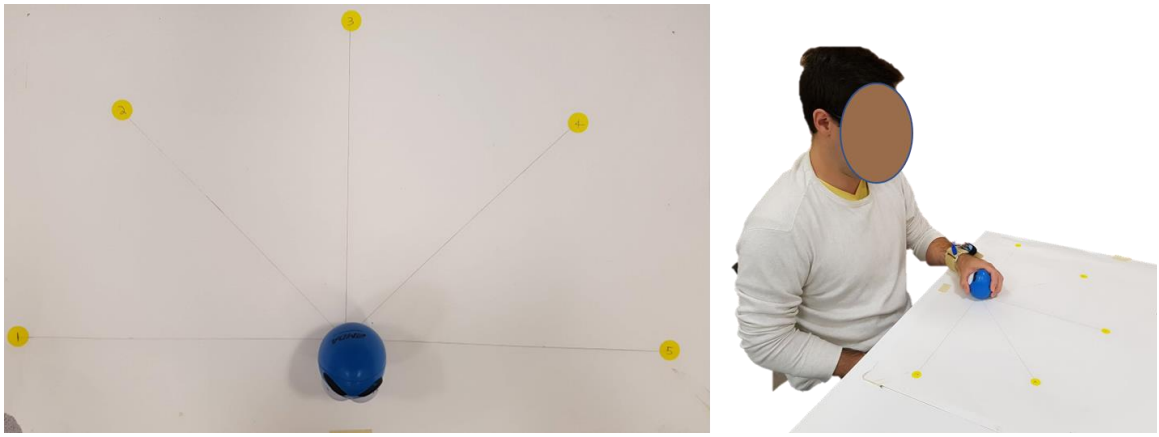

Figure 4.1. Testing area : (a) 5 positions for reaching task, (b) participant seated in a chair for grasping tasks.

4.2.3. Instructions to Participants

Participants were briefed on the details of the study and then signed an informed consent form. The ethics of this study were approved by Simon Fraser University. Participants were then fitted with the device, given a demonstration of the motions to be performed, and then asked to follow the exercise prompts on the computer screen via a LabVIEW interface.

The LabVIEW VI interface received data from the device, saved it to the computer disk, and had a graphical user interface (GUI) which prompted the user to complete each action with an on-screen message. Motions were completed in 10 repetitions; the task order for each repetition was pre-generated with a seeded (pre-determined) random shuffle. A test supervisor was present to monitor the testing and managed the data acquisition in accordance with university research ethics.

4.3. Data Pre-Processing, Feature Calculation, and Statistical Tests

A description of data pre-processing, feature extraction and statistical tests are discussed below.

4.3.1. Pre-processing

Data analysis of the system (data cleansing, treatment, and classification) is summarized below. Data were median filtered to smooth high frequency components before secondary features were calculated for each sensor channel. The median filter was selected instead of the average filter because of its improved ability to remove noise signals. The 3 point median filter introduces a 17-millisecond delay based on the 12 Hz data recording frequency, but this was not a concern for the moderate speed movements of this study, which were analyzed in an offline model. The resulting data were combined

across participants and normalized before training. Each participant completed 24 actions with 10 repetitions, resulting in 240 trials, Figure 4.3. The secondary features compressed the time series data into a single row per trial, resulting in 240 rows of data per participant. The process of data recording, data treatment, classifier training, and testing is described below.

1. Calculate the spatial average of thermal sensor data
2. Smoothing: Apply median filter data (window size = 3)
3. Apply secondary features (7 calculations, described in Table 4.2) to each input channel
4. Normalize features
5. Evaluate with different machine learning classifier models. Select an optimal model based on accuracy and processing time

The description below describes the treatment of raw sensor data and the calculations of the secondary features. Raw data included accelerometer, gyroscope, and quaternion from the IMU, as well as thermal data from the Omron D6T sensor. Quaternion is a four-dimensional number composed of a scalar and vector component and is used to represent orientation in 3D space [39]. The quaternion representation of orientation is typically favoured over the Euler representation since the Euler representation can suffer from gimbal lock [40] when 90 degree rotations are performed about an axis [41]. Quaternion was calculated by the main microcontroller using the Mahony complementary filter [42] to reduce integration drift in the orientation calculation. Magnetometer data, the filtered accelerometer data, and filtered gyroscope sensor data were input to the complementary filter. Raw magnetometer data was not directly used as input to the classification model due to its sensitivity to electronics and metals in the environment and its lower 8 Hz update rate. The accelerometer measures, in each of its 3 mutually orthogonal sensors axes, the vector of the gravitational field and linear acceleration resulting from forces acting on the sensor [38]. The acceleration values recorded from the IMU were normalized relative to the average Earth gravity force of 9.81 m/s2. The

gyroscope sensor measures angular velocity about each of its 3 mutually orthogonal axes and is converted to degrees per second values for our investigation. Thermal sensor data were averaged in a row-wise, column-wise, and quadrant-wise manner to reduce the number of input features to the model and increase processing speed, resulting in 12 primary features from the thermal sensor. Raw accelerometer and gyroscope data were filtered with a 42 Hz digital low-pass filter that is built-in to the MPU9250 IMU's central processor [33]. 22 primary features were obtained from the 3 axes of the accelerometer, 3 axes of the gyroscope, 4 quaternions, and 12 values from the thermal sensor.

Seven secondary features were calculated for each of the primary features (Table 4.2). These secondary features have previously demonstrated strong performance in high accuracy motion classification in Zhang et al [18]. These 7 secondary features were applied to each of the 22 primary features, producing 154 secondary features. An example image of feature processing for 3 different motions (Bobath handshake, Horizontal Shoulder Extension, and Pick up the phone) is shown in Figure 4.2; each row is a different motion and each column is a processing step. Note that the median filter will smooth some of the high frequency components and peaks that are visible in the raw data. Four machine learning models were then applied to the secondary features: Linear Discriminant Analysis (LDA), Support Vector Machine (SVM), K-Nearest Neighbours (KNN), and classification trees. These four machine learning models were selected for analysis because their prevalence in existing motion classification studies allows some aspect of comparison: LDA ([43,44],[45],[46], [47], [48]), SVM([18][43][49][44][47][13]), KNN([18] [50][47][13,48]), and Classification trees([8,13,51,52]).

Table 4.2. Summary of secondary features calculated on each sensor channel.

#	Secondary Feature	Calculation notes
1	Mean	Mean value of each channel for a single motion
2	Standard Deviation	Standard deviation of each channel
3	Duration	Number continuous samples above 20th percentile value for the motion
4	Energy	The squared sum of the data sequence
5	Dominant frequency power	The peak power of the Power Spectral Density (PSD), calculated with periodogram function in MATLAB
6	Dominant frequency	The peak frequency of PSD
7	Mean Power	The average power of PSD

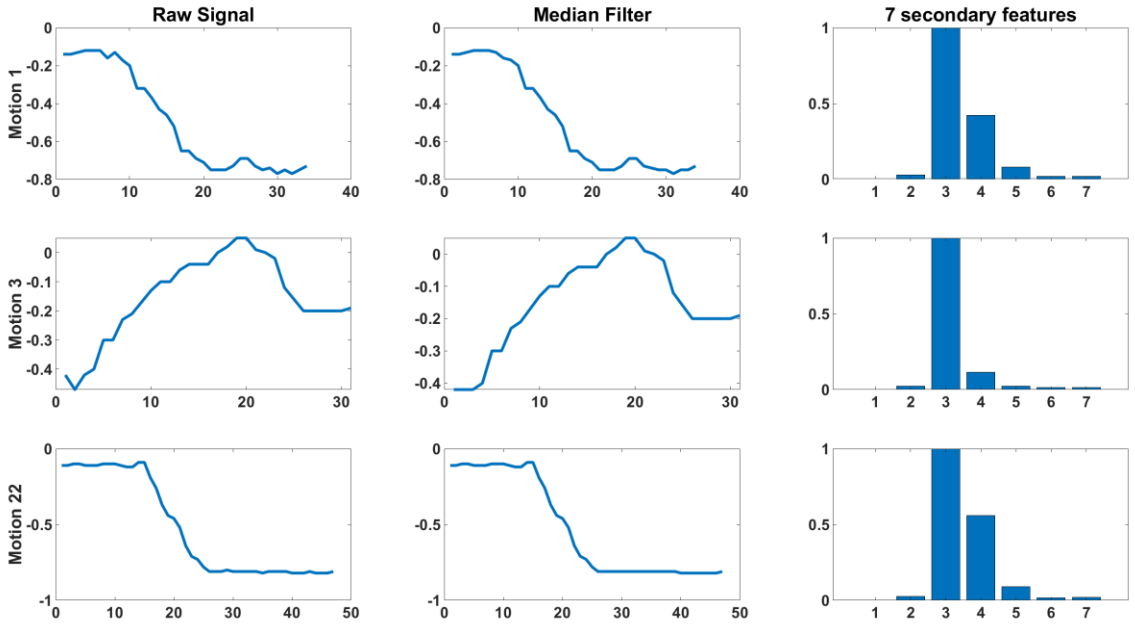

Figure 4.2. Signal processing steps for 3 different motions. Each row is a different motion. Each column shows a processing step.

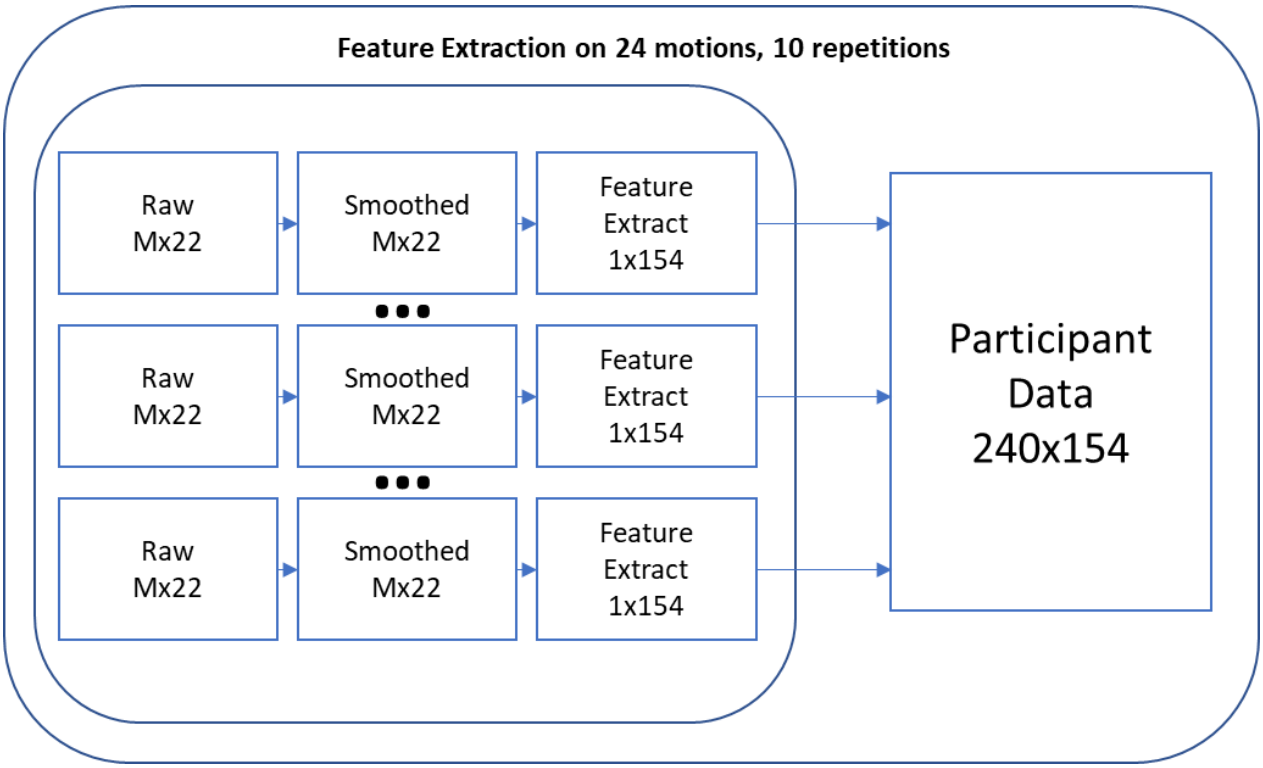

Figure 4.3. The feature extraction process for the 24 motions and 10 repetitions of a participant's trial data.

4.3.2. Statistical analysis

Paired statistical tests [97] were used to assess significance between distributions. The normality of data distributions was assessed with the Shapiro-Wilk test and Q-Q plots where required. Distribution residuals that appeared normal at a p=0.05 significance were tested with a parametric t-test for the single paired test or one-way ANOVA for multiple comparisons. Distributions that did not appear to have normal residuals were analyzed with Wilcoxon signed rank test for the single paired test or Kruskal Wallis for multiple comparisons. Each of these statistical evaluations was completed in MATLAB 2018a with a default significance value of p=0.05. MATLAB built-in functions ttest, anova1, signrank and kruskalwallis were used.

4.4. Chapter Conclusion

A description of the study that was conducted with 11 healthy participants was described, including a description of the 24 motions performed, the test workspace, and the instruction is given to the participants. Data processing, secondary feature calculation, and statistical analysis were also described.

The protocol was designed to explore the performance of the proposed system by evaluating classification accuracy for a set of 24 motions. This description of a study to evaluate system performance supports Objective 2.

Chapter 5.

Results and Discussion

This chapter explores system performance in support of **Objective 2** and the performance contribution of the thermal sensor in support **Objective 3**. The chapter is organized as follows: Machine learning model performance is compared in 5.1, and personalized and generalized classification models are compared in 5.2. Contributions of this work in comparison to prior work are discussed in section 5.3. Discussions of system performance in different directions are discussed in 5.4 and performance based on training data volume is discussed in 5.5. The performance of the thermal sensor is presented in 5.6. The chapter is concluded in 5.7.

5.1. Performance of Machine Learning Models

A comparison of machine learning models was assessed by completing the personalized model evaluation in a randomly shuffled, stratified 10-fold cross validation, ensuring that sufficient test data was present in each fold. A visualization of the training and testing process is shown in Figure 5.1. Note that the process shown is repeated 10 times for each participant to minimize outliers that might result due to the shuffling of the data.

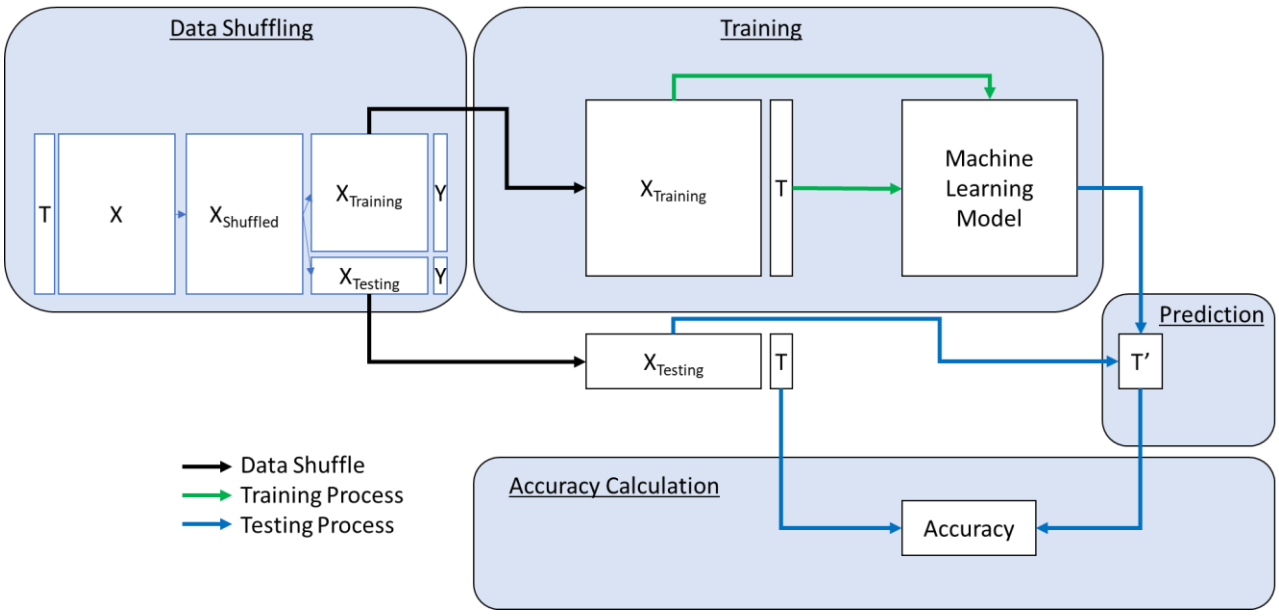

Figure 5.1. Machine Learning model testing and training process. The data (X) and labels (T) have been segmented into training and testing data.

Machine learning models were evaluated on this dataset and the mean accuracy and processing times were compared (Table 5.1). Personalized models were evaluated on each participant 10 times by shuffling the data each time, selecting 90% of the data for model training and 10% for model testing. Classification accuracy was reported for each of the 10 iterations and the average classification accuracy for that participant was calculated across the 10 iterations. The overall average classification accuracy was then calculated by taking the average of the 11 participant averages. This was repeated for each of the machine learning models in Table 5.1. The average time required for the model to classify a set of 24 motions was calculated by averaging the 10 classification times from a participant's 10 iterations and then taking the average of the 11 participants' times.

Table 5.1. Model performance with a personalized classification model.

Model	Average Accuracy, IMU + Thermal Spatial Average (N=11)(%)	Average time to classify a set of 24 motions, (s)

SVM	90.61	4.06
KNN (neighbourhood 1)	74.15	0.04
LDA	93.55	0.28
Classification Trees	82.08	0.65
Neural Network	75.80	0.009

While the primary criterion for the optimum classifier was high classification accuracy, the short processing time is an additional consideration since a future system might incorporate online classification. An online classifier would benefit from short classification times so that real-time information might be delivered to the user. LDA was selected as an optimum model due to its highest accuracy and fast processing time relative to the other evaluated models (Table 5.1). The SVM model would be less suitable for online classification due to its much slower classification time.

During each training and testing of the classifier model, the time required to classify all 24 motions was recorded. The average time was then calculated for each classifier model, across each of the participants. The 0.28 second average classification time for the LDA model indicates that online classification of motions could be feasible. A faster classification time is of interest for the future development of the system where online classification could be used to provide coaching or feedback to the user.

While the KNN and Neural Network classifiers had the fastest processing times, their classification accuracies were the poorest. Conversely, SVM yielded considerably high classification accuracy, but suffered from much slower processing times.

Standard built-in MATLAB models were employed for this analysis, although parameters for each model were briefly tuned to improve classification accuracy. The KNN model accuracy was highest with a neighbourhood size of 1, and LDA accuracy was highest with a pseudo linear discriminant instead of a linear discriminant.

Additionally, Principal Component Analysis (PCA) [63] was applied to each model to examine opportunities for a reduced feature space [98]. It was found that PCA could transform the feature space to represent 99.5% of the original variance with a feature reduction from 154 to 60 features with an only marginal decrease in accuracy and a slightly decreased processing time.

The highest average classification accuracy was 93.55 ± 5.1%, (N=11); this was obtained by training personalized LDA classifier models to each participant. A confusion matrix shows the correctly and incorrectly classified actions for each task for the combined results of the personalized model evaluation, (Figure 5.2). The actual motion performed is viewed in the x axis (Target) while the motion predicted by the classifier is displayed in the corresponding row. The colour map also indicates the relative score of each cell, on a scale from 0 to 110. Since 11 participants performed each motion 10 times, a perfect score for that motion would be a value of 110 in the diagonal of this matrix.

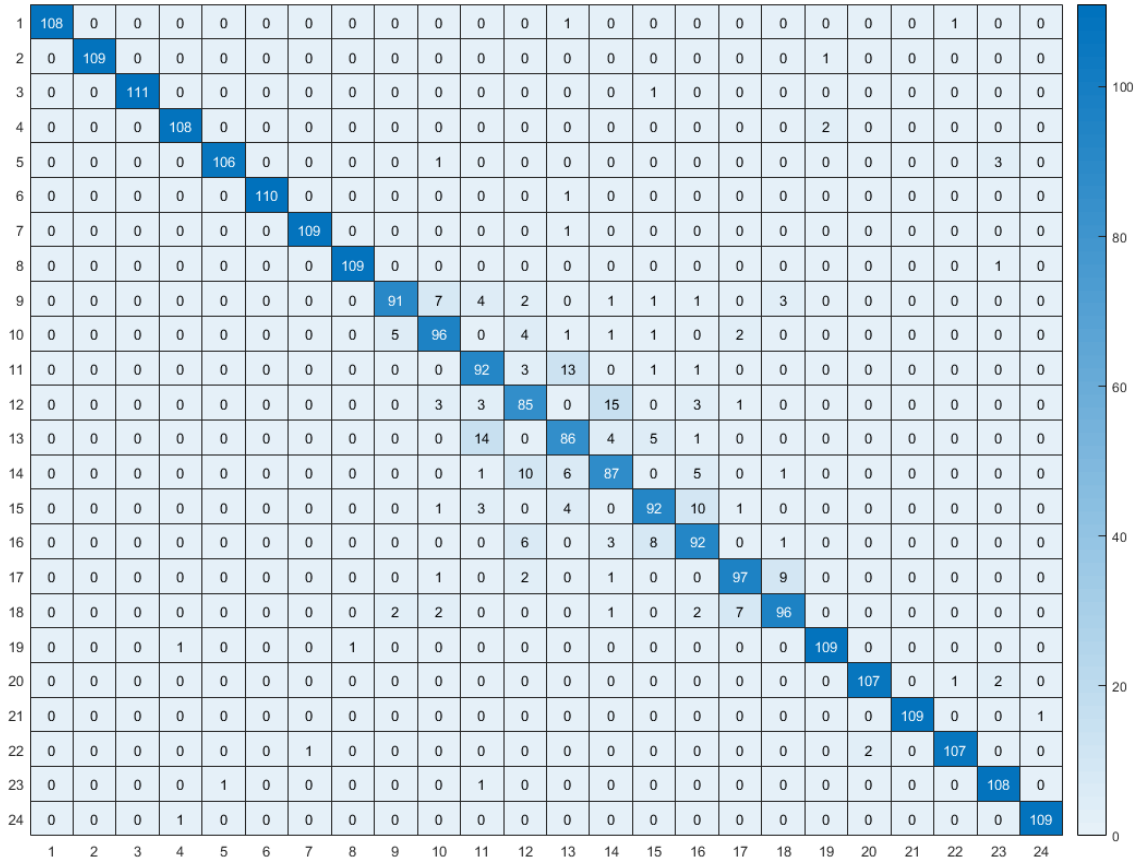

Figure 5.2. Confusion matrix for LDA model classifier with 11 healthy people. Target motion is shown on the x axis and predicted motion on the y axis

5.2. Personalized and Generalized model performance

The generalized model classification performance was evaluated as follows: A machine learning model was trained on data from 10 participants, and then the machine learning model was tested on the 11th participant, whose data had not been inputted into the model. This was completed 11 times, using a different participant for the model testing each time and the remaining 10 participants' data for training the model. In each iteration, classification accuracy was calculated for the model's ability to classify the motions of that participant. The resulting average classification accuracy was 82.5 ± 10.1% (N=11). A generalized model that can accurately classify a user's actions without prior training on that user's data could be beneficial in scenarios where motion classification is needed

quickly, or when a user is unable to participate in training the classification model. This could be useful in a rehabilitation scenario where a patient might be unable to complete an entire exercise regimen due to fatigue, yet the classification of exercise motions is still desired.

The personalized classification model represents the expected performance for a system that is trained on data from an individual user and then tested on newly recorded data from that individual. This accuracy (93.55% with the personalized LDA model, Section 5.1) is expectedly higher than generalized model training since the data was consistently recorded on the single user with the band worn only once. A rehabilitation patient with sufficient mobility to complete exercises independently in an outpatient rehabilitation session could train a personalized classification model and possibly have their exercise motions classified with similarly high accuracy. However, it should be noted that the patient's mechanics of movement may change as they progress through rehabilitation, and the sensor data may change as a result. This system's classification accuracy compares favorably to accuracies reported in existing work with fewer motions (91-99% accuracy for up to 8 motions, [81], [84], [99]). The confusion matrix shows that a greater number of misclassifications were observed for motions 9-18, which correspond to the table-top reaching exercises (Figure 5.2).

The generalized classification model performance was strong considering that the model had not been exposed to any of the participant's data during training. This indicates that the system has the potential to adapt to new users when the device is worn in a similar manner to the previous users. A system that is used properly could yield up to 82% prediction accuracy on 24 motion classes without any prior training by that user. This performs similarly well to Zinnen et al [75], which proposed a 2-device system with a device on each wrist; 20 motions were classified in a similar evaluation. They obtained

82% accuracy and increased their accuracy to 86% when a validation step was introduced to reject motions that did not match the anatomical capabilities of a typical person. Comparatively, our 1-device system resulted in a classification accuracy of 93.55% for 24 motions. The high classification accuracy of the healthy participants' personalized classification models prompts further investigation into the possibility of training a personalized prediction model for a rehabilitation patient. Future development of this system should also consider using knowledge of human anatomical constraints to reject unlikely motions and arm poses and likely increasing classification accuracy.

The system's classification accuracy is 93.55% with personalized classification models and 82.5% with generalized classification models. The strong performance of the generalized models could allow the classification of a user's motions when the model is not trained on the user's data. The device could thus be useful for classification even when the user cannot physically participate in classifier model training. Since the classifier can be trained on other users and evaluated with reasonable accuracy, this may indicate that users perform rehabilitation motions with some degree of similarity (at least in the scope of the sensor data examined). A generalized classifier model can be generated with more training data than a single user can feasibly provide. The larger volume of training data available to the generalized model might improve the model's ability to predict movements on a wider portion of the population.

5.3. Performance Relative to Prior Work

Comparing the performance of the system to similar existing work provides a perspective on the contributions of this work. Classification accuracy of 93.55% was obtained on 24 arm rehabilitation motions in this performance evaluation using the personalized classification models.

In comparison, the literature review indicated two benchmarks for state-of-the-art systems using single-device wearables for arm motion tracking. 4 arm motions were classified in a study of 8 motions with a healthy population in Yang et al [84], resulting in a 95% accuracy. Further, 6 arm motions were classified in a study with a stroke survivor population in Zhang et al [63], resulting in a 99.4% classification accuracy.

The results of this system's performance evaluation demonstrate a 300% increase in the number of arm motions that can be classified (Table 5.2) while maintaining similar classification accuracy levels. This directly supports the performance evaluation goal of Objective 2. Further, the contributions of this performance evaluation classified arm motions from 4 different rehabilitation protocols, while the current state-of-the-art studies each classify motions from a single rehabilitation protocol.

Table 5.2. System Performance in comparison to the current state of the art

	State-of-the-art for single-device arm motion classification [81] [82] [83] [84] [63]	**Result in this thesis**	**Performance Increase or Decrease (%)**
Number of arm motions classified	6	24	300
Number of rehabilitation exercise protocols	1	4	300

5.4. Direction and Spatial Performance

It was observed that individual classification accuracies for the 10 table-based reaching motions (motions 9-18) were lower than the other 14 motions as evidenced by the misclassifications visible in the off-diagonal of the confusion matrix, Figure 5.2. As a result, the accuracy of different movement directions was examined. It was found that the performance was significantly correlated to the reaching angle, $F(4,105)=48.54$, $p < 0.05$.

Specifically, movements reaching to the right were most accurate, and movements reaching to the left were least accurate. One possible explanation for this observation is that reaching motions to the right with the left hand will cause more of the body to be visible in the thermal sensor FOV, resulting in an improved ability to sense the wrist orientation relative to the body and thus allow more accurate classification of motions. Conversely, arm movements to the left may move to positions where the thermal sensor is pointing away from the body. The thermal sensor might be unable to detect the participant within its FOV if the participant rotates their shoulder outward during the reaching action. Completing this study with the device worn on the right arm would likely yield the opposite trend. For future development, the device design could be further refined to ensure the thermal sensor is positioned optimally for the specific motions being classified. Reaching direction (forward or backward) was not found to significantly correlate to performance, $F(1,20)=2.51$, $p=0.129$.

5.5. Performance with Reduced Training Data

An investigation into system accuracy with minimal training data was also performed. In this investigation, the machine learning model was trained and tested on

each of the 11 users. The model was tested on the last 3 recorded repetition sets, but the number of datasets input to model training was varied from 2 to 7 sets. It was observed that the system performs well with a reduced set of training data; training on 4 repetition sets is sufficient to yield an average classification accuracy of 83% (Figure 5.3). This finding indicates that training a personalized machine learning model for a user with 4 repetition sets of motions could yield up to 83% classification accuracy. While a larger amount of training data would be preferred to further increase classification accuracy, additional data recordings might be difficult due to patient fatigue in the clinical rehabilitation session.

The system's ability to classify 24 motions with only 4 training recordings and maintain acceptable performance indicates that it can be quickly trained, thus possibly improving the accessibility and efficiency of rehabilitation delivery.

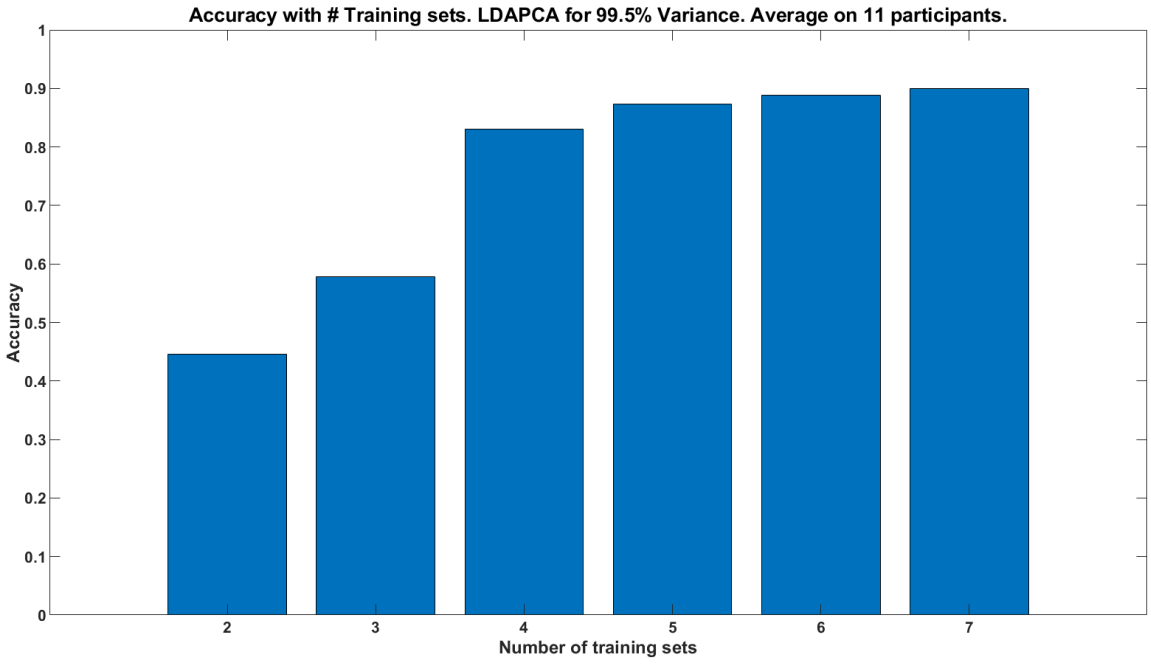

Figure 5.3. Classifier accuracy as a function of the number of training sets. Accuracy is evaluated on 3 data recordings for each participant. Average accuracy is calculated across the 11 participants.

5.6. Performance Contribution of the Thermal Sensor

The classifier was evaluated twice to examine the performance contribution of the thermal sensor: once IMU only and once with features that were derived from both the IMU and thermal sensor. It was observed that the addition of a thermal sensor contributed to a significant increase in accuracy, from 75 ± 4% to 93.55 ± 4%, (F(1,20)=90.53, p=7.25e-09), Figure 5.4.

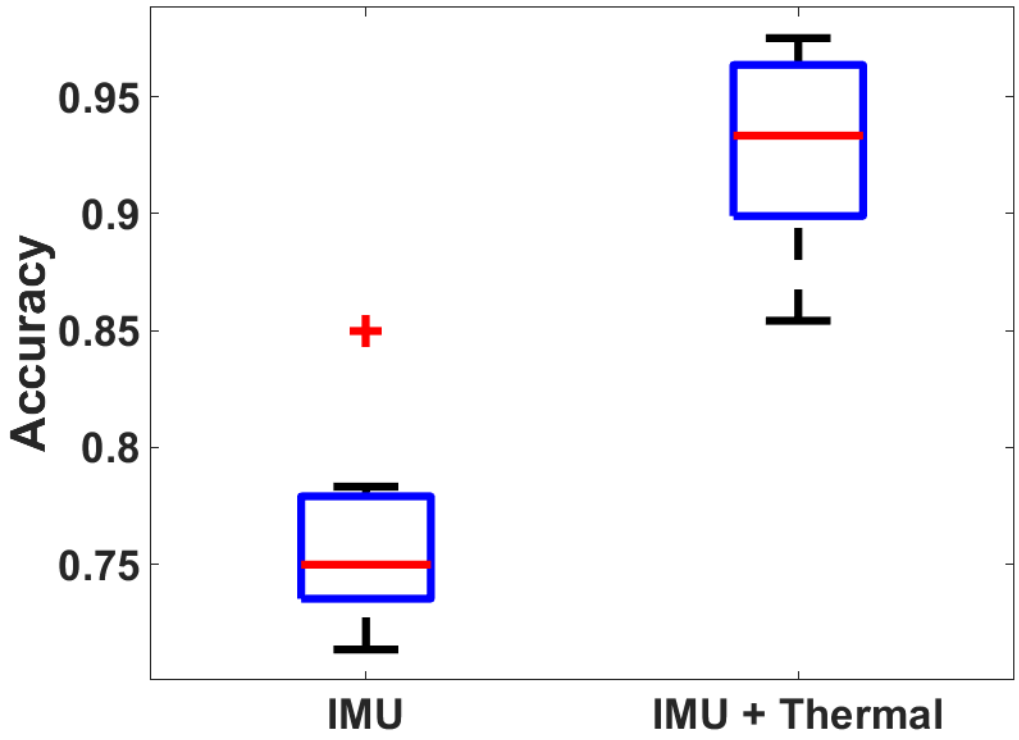

Figure 5.4. Accuracy comparison for IMU and IMU + thermal sensor

Classification accuracy for secondary features from each sensor (accelerometer, gyroscope, and thermal sensor) was compared to each other. The thermal sensor-based features provided significantly higher accuracy than gyroscope-based features (p=0.04). The thermal sensor appears to have provided a stronger performance than accelerometer-based features but the difference is not significantly different, (p=0.28), Figure 5.5.

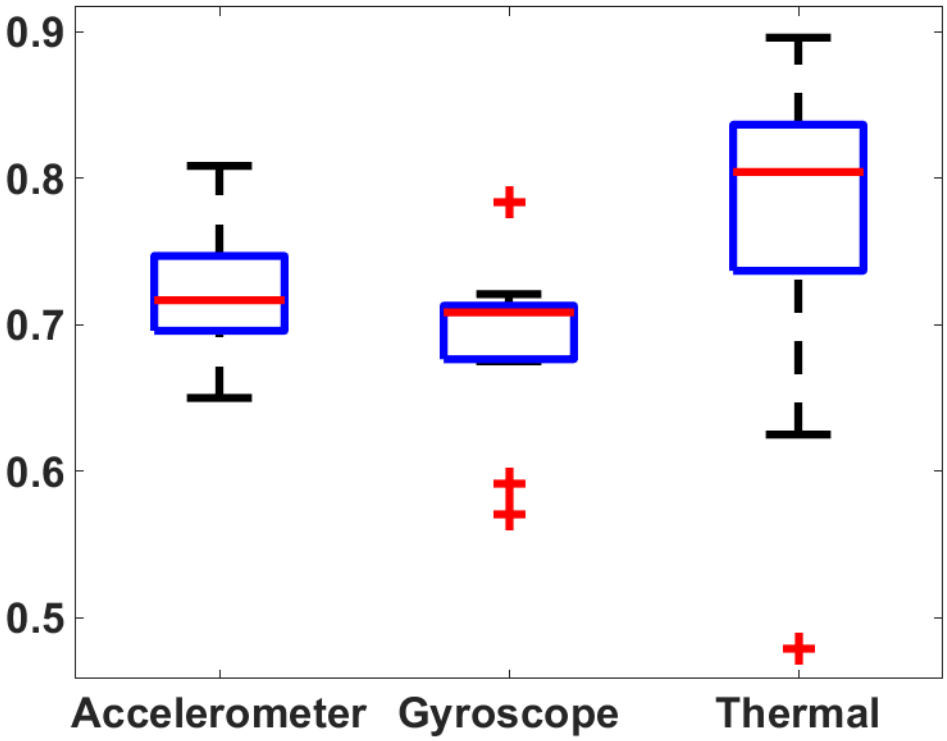

Figure 5.5. Classifier performance comparison for each sensor: accelerometer, gyroscope, and thermal sensor

The preliminary study into sensor hardware selection indicated that the thermal sensor's raw data channels contributed more strongly to classifier performance than the accelerometer and gyroscope sensors for classifying 22 static poses [90]; a similar trend is observed in this study for classifying 24 arm motions [100]. The median accuracy of the thermal sensor (80% accuracy) array is higher than the classification accuracies of the accelerometer or gyroscope sensors. This reiterates that the thermal sensor provides valuable data to aid in arm motion classification.

While this study applied the same set of feature calculations to each sensor, a future investigation could determine the highest performing features for each sensor and propose specialized features to maximize the contribution of each sensor. Additionally, the data transmission rate of the system could be increased if the number of primary features (sensor channels) was reduced or if onboard motion classification was introduced

to remove the need for wireless transmission of primary feature data to a processing computer. The increased operating frequency of the system may provide an opportunity to increase classification accuracy. However, Gao et al [101] and Krause et al [102] note that the classification accuracies increase marginally with an increased sampling rate while decreasing the battery life of the system. Future work will expand on this examination of feature selection and determine the effects of sampling rate on classification accuracy.

5.7. Chapter Conclusion

The performance of the proposed device was explored in support of **Objective 2** and **Objective 3**. The classification accuracy of 93.55% for 24 motions greatly increases the number of arm motions that can be classified by a single-device system. This single-device system for arm motion classification exceeded the number of arm motions classified by previously presented systems found in the literature. Processing times are as low as 11 milliseconds per motion, indicating that real-time activity classification could be feasible with the current hardware. Furthermore, the performance of the classifier remains strong at 82% when a generalized model is trained, allowing a user's activity to be classified without any user training. The personalized model can function well with minimal training, yielding 83% accuracy after 4 training recordings. These findings satisfy **Objective 2**.

The addition of the thermal sensor provides a significant improvement in classification accuracy for a single-device system that classifies 24 arm motions, satisfying **Objective 3**. The classification accuracy of the thermal sensor is significantly higher than the gyroscope sensor but not significantly higher than the accelerometer sensor. Since the combined performance of the thermal and inertial sensors outperforms the individual sensors, it is possible that the sensors complement one another in increasing classification

accuracy. This determination of the performance contribution of the thermal sensor satisfies Objective 3.

In this chapter, a study with 11 healthy participants found that the proposed system can classify arm motions in a reasonable time and with comparable accuracy to existing studies, while greatly exceeding the number of arm motions that can be classified. The results presented in this chapter clearly satisfies **Objective 2** and **Objective 3**.

Chapter 6.

Conclusions

This chapter provides a summary of the findings of this thesis and an outline of areas of future research. In section 6.1 the thesis objectives are recalled, and findings are summarized in support of each objective. Future work is discussed in section 6.2.

6.1. Conclusion

Although there are several technologies available for motion tracking, they are ineffective, intrusive, or cumbersome to wear. Compared to these alternatives, single-device, body-mounted wearable are more portable, affordable, and convenient choices for an activity monitoring device. However, using a single-device wearable decreases the number of motions that can be successfully classified compared to multi-device systems. Thus, there is a strong need to improve the performance of single-device wearable systems in regards to the number of arm motions that can be classified.

In this study, an infrared sensor was successfully introduced into a single-device wearable and was able to classify a greater number of arm motions than is currently reported in the literature. The device developed in this study was able to classify 24 arm motions, compared to 6 arm motions previously reported literature. Additionally, the increased classification accuracy resulting from the thermal sensor addition was determined to be statistically significant.

Objective 1 of this work was to *develop a single-device arm motion classification system to classify a larger number of arm motions than prior systems identified in the literature*. A single-device wearable system was proposed and built. This system

incorporated an infrared sensor, accelerometer, and gyroscope sensor. The device was positioned appropriately on the wrist to reduce the influence of vibrations, and the infrared sensor was positioned proximally on the device, pointing inwards toward the user to capture the user's torso in the most common arm orientations. The sensor hardware selection and hardware design of the final system were described in Chapter 3 and software code is documented in Appendix C. The sensor selection, sensor layout, hardware design, and software design satisfy Objective 1.

Objective 2 was to *perform a preliminary investigation on the performance of the system in a study of 24 arm motions, with healthy volunteers, in a controlled environment*. The methods to evaluate the system performance with 11 healthy participants were described in Chapter 4. The results were described in Chapter 5 where the system classified 24 arm motions with 93.55% accuracy using an LDA model. This performance relative to current literature represented a 300% increase in the number of arm motions that can be classified with a single-device wearable. Generalized model accuracies of 82.5% indicated that the device classified arm motions on a healthy participant without prior training, demonstrating that the device could be quickly deployed for activity classification with minimal user configuration. The device allowed an 83% classification accuracy for a personalized model in 4 recordings, indicating that accurate classification could be obtained with minimal model training. The performance of this device and the considerable increase in performance relative to existing work satisfy Objective 2.

Objective 3 was to *perform a preliminary investigation on the performance contribution of the thermal sensor, with healthy volunteers, in a controlled environment*. The addition of the infrared sensor was found to significantly increase accuracy from 75 to 93.55%, ($F(1,20) = 90.53$, $p < 0.05$) in 5.6, satisfying Objective 3. Furthermore, the infrared sensor was found to allow significantly higher classification accuracy than the

gyroscope sensor ($p < 0.05$) for the classification of 24 arm motions. The thermal sensor also delivered higher classification accuracy than the accelerometer sensor, but this difference was not statistically significant.

6.2. Limitations

The performance evaluation of this system was examined in a preliminary study with healthy participants in a controlled environment. It is possible that the classification accuracy of this system may decrease in an uncontrolled environment or when used with a different population. Specifically, since stroke impairment can affect the smoothness of movement, movement speed, and muscle strength [103] [104], it is possible that the classification of stroke survivor movements may be more difficult than a healthy person's motions since these impairments might affect the consistency of movement. A rehabilitation patient might also perform the motion differently at various times throughout their rehabilitation, adding further variability to the recorded data.

The classification performance might decrease if the device is removed and donned again between training and testing sessions. However, the performance of the generalized model indicates that the device can continue to function when donned and removed; the device was donned and removed 11 times by different participants during this evaluation and performed well.

6.3. Future Work

The high accuracy with which this system could classify motions prompts the need for future evaluation of the system with stroke-affected individuals in a controlled environment and a subsequent study with stroke-affected individuals in a home environment. Future investigation should also consider machine learning model

differences between healthy and affected populations and explore if a hybrid model could represent both populations.

Further development of this system should be applied to more specific scenarios, such as allowing home-based rehabilitation to be more easily monitored by clinicians by facilitating remote access to patient activity data. These sensor arrangements could be developed into customized garments or attached to everyday objects to easily record user motions throughout the home, which is similar to the work described in Tavares et al [105] or incorporated into video games to provide motivation and feedback to the participant, as described in Bento et al [106]. Future development should also focus on methods to quantify the quality of motion performed; one such method proposed in Bento et al [106] defined motion quality by comparing a recorded motion to an expected range-of-motion.

Integration to secure cloud storage could allow patient exercise data to be delivered remotely to clinical experts. Patient exercise data could be locally recorded through a custom application on an Android or iOS smartphone, which can connect to the device via Bluetooth connection. This information could then be uploaded to a secure online platform via a Wi-Fi connection and then accessed by clinical professionals. Future development would be required to develop the smartphone application, integration to a secure file storage service, and user-interface for stakeholders to view the patient's exercise data.

While a reasonably high classification accuracy was achieved on the data that was collected over a period of 3 weeks, future work should examine the performance of the system in long-term operation and examine the effects of sensor drift. Additional filtering or kinematic constraints might be required to maintain robust operation in these situations.

Additionally, future work should further explore and compare the performance of the generalized and personalized classification models. It is possible that a hybrid solution between the personalized and generalized models might provide benefits in a clinical environment. In a hybrid model scenario, a pre-trained, generalized classification model could allow a patient's motions to be quickly classified while requiring minimal training data from the user. The model could become personalized over time by incorporating data from the patient.

Chapter 7. References

[1] X. Li, O. W. Samuel, X. Zhang, H. Wang, P. Fang, and G. Li, “A motion-classification strategy based on sEMG-EEG signal combination for upper-limb amputees,” *J. Neuroeng. Rehabil.*, vol. 14, no. 1, pp. 1–13, 2017.

[2] P. Jung, S. Member, G. Lim, and S. Kim, “A Wearable Gesture Recognition Device for Detecting Muscular Activities Based on Air-Pressure Sensors,” *IEEE Trans. Ind. Informatics*, vol. 11, no. 2, pp. 485–494, 2015.

[3] A. Bulling, U. Blanke, and B. Schiele, “A tutorial on human activity recognition using body-worn inertial sensors,” *ACM Comput. Surv.*, vol. 46, no. 3, pp. 1–33, 2014.

[4] O. D. Lara and M. A. Labrador, “A Survey on Human Activity Recognition using Wearable Sensors,” *IEEE Commun. Surv. Tutorials*, vol. 15, no. 3, pp. 1192–1209, 2013.

[5] A. Mannini and A. M. Sabatini, “Machine learning methods for classifying human physical activity from on-body accelerometers,” *Sensors*, vol. 10, no. 2, pp. 1154–1175, 2010.

[6] C. C. Yang and Y. L. Hsu, “A review of accelerometry-based wearable motion detectors for physical activity monitoring,” *Sensors*, vol. 10, no. 8, pp. 7772–7788, 2010.

[7] R. S. Falck, J. R. Best, M. C. R. Li, J. J. Eng, and T. Liu-Ambrose, “Revisiting the MotionWatch8©: Calibrating Cut-Points for Measuring Physical Activity and Sedentary Behavior Among Adults With Stroke,” *Front. Aging Neurosci.*, vol. 11,

no. August, pp. 1–12, 2019.

[8] R. S. Falck *et al.*, “Sleep and cognitive function in chronic stroke: A comparative cross-sectional study,” *Sleep*, vol. 42, no. 5, 2019.

[9] S. Patel, H. Park, P. Bonato, L. Chan, and M. Rodgers, “A review of wearable sensors and systems with application in rehabilitation,” *J. Neuroeng. Rehabil.*, vol. 9, no. 1, p. 21, 2012.

[10] R. Teasell, “Background Concepts in Stroke Rehabilitation,” pp. 1–48, 2016.

[11] J. H. Rimmer, “Barriers associated with exercise and community access for individuals with stroke,” *J. Rehabil. Res. Dev.*, vol. 45, no. 2, pp. 315–322, 2008.

[12] C. Chen, P. S. Neufeld, C. A. Feely, and C. S. Skinner, “Factors influencing compliance with home exercise programs among patients with upper-extremity impairment,” *Am. J. Occup. Ther.*, vol. 53, no. 2, pp. 171–180, 1999.

[13] J. Daly, A. P. Sindone, D. R. Thompson, K. Hancock, E. Chang, and P. Davidson, “Barriers to participation in and adherence to cardiac rehabilitation programs: a critical literature review.,” *Prog. Cardiovasc. Nurs.*, vol. 17, no. 1, pp. 8–17, 2002.

[14] H. Zhou and H. Hu, “Human motion tracking for rehabilitation-A survey,” *Biomed. Signal Process. Control*, vol. 3, no. 1, pp. 1–18, 2008.

[15] E. Henricksen Burkow, T., Johnsen, E., & Vognild, L., “Privacy and information securityrisks in a technology platform for home-based chronic disease rehabilitation and education,” *BMC Med. Inform. Decis. Mak.*, vol. 13, no. 1, pp. 1–13, 2013.

[16] P. Miller, C. K. Gowland, J. Griffiths, P. Stratford, and R. Barclay-goddard, “Chedoke-McMaster Stroke Assessment,” 2008. [Online]. Available: https://www.sralab.org/sites/default/files/2017-07/CMSA Manual and Score Form.pdf. [Accessed: 21-Mar-2018].

[17] S. Barreca, “CAHAI Chedoke Arm and Hand Inventory Administration guidelines version 2,” 2012. [Online]. Available: http://www.cahai.ca/layout/content/CAHAI-Manual-English-v2.pdf. [Accessed: 21-May-2018].

[18] J. Eng and J. Harris, “Graded Repetitive Arm Supplementary Program Exercise manual Levels 1-3.” [Online]. Available: http://strokerecoverybc.ca/wp-content/uploads/2011/11/GRASP_All_3_levels11490.pdf. [Accessed: 01-May-2018].

[19] U. Maurer, A. Smailagic, D. P. Siewiorek, and M. Deisher, “Activity recognition and monitoring using multiple sensors on different body positions,” in *International Workshop on Wearable and Implantable Body Sensor Networks*, 2006.

[20] K. Van Laerhoven and O. Cakmakci, “What Shall We Teach Our Pants ?,” 2000.

[21] X. Fan, H. Zhang, C. Leung, and C. Miao, “Comparative study of machine learning algorithms for activity recognition with data sequence in home-like environment,” in *IEEE International Conference on Multisensor Fusion and Integration for Intelligent Systems*, 2017, pp. 168–173.

[22] M. J. Akhlaghinia, “Occupancy Monitoring and Prediction in Ambient Intelligent Environment,” no. October, 2010.

[23] P. Hevesi, S. Wille, G. Pirkl, N. Wehn, and P. Lukowicz, “Monitoring household

activities and user location with a cheap, unobtrusive thermal sensor array," pp. 141–145, 2014.

[24] P. H. Veltink, H. B. J. Bussmann, W. De Vries, W. L. J. Martens, and R. C. Van Lummel, "Detection of Static and Dynamic Activities Using Uniaxial Accelerometers," vol. 4, no. 4, 1996.

[25] W. J. Kang, J. R. Shiu, C. K. Cheng, J. S. Lai, H. W. Tsao, and T. S. Kuo, "The Application of Cepstral Coefficients and Maximum Likelihood Method in EMG Pattern Recognition," *IEEE Trans. Biomed. Eng.*, vol. 42, no. 8, pp. 777–785, 1995.

[26] X. Yong and C. Menon, "EEG classification of different imaginary movements within the same limb," *PLoS One*, vol. 10, no. 4, pp. 1–24, 2015.

[27] L. Liao, D. Fox, and H. Kautz, "Location-based activity recognition using Relational Markov Networks," *IJCAI Int. Jt. Conf. Artif. Intell.*, pp. 773–778, 2005.

[28] M. Buettner, R. Prasad, M. Philipose, and D. Wetherall, "Recognizing daily activities with RFID-based sensors," *ACM Int. Conf. Proceeding Ser.*, pp. 51–60, 2009.

[29] Q. Wang, P. Markopoulos, B. Yu, W. Chen, and A. Timmermans, "Interactive wearable systems for upper body rehabilitation: a systematic review," *J. Neuroeng. Rehabil.*, vol. 14, no. 1, p. 20, 2017.

[30] S. O. H. Madgwick, A. J. L. Harrison, and R. Vaidyanathan, "Estimation of IMU and MARG orientation using a gradient descent algorithm," in *IEEE International Conference on Rehabilitation Robotics*, 2011, pp. 179–185.

[31] H. Zhao and Z. Wang, “Motion measurement using inertial sensors, ultrasonic sensors, and magnetometers with extended kalman filter for data fusion,” *IEEE Sens. J.*, vol. 12, no. 5, pp. 943–953, 2012.

[32] M. Kok, J. D. Hol, and T. B. Schön, “Using Inertial Sensors for Position and Orientation Estimation,” *Found. Trends Signal Process.*, vol. 11, no. 1, pp. 1–153, 2017.

[33] S. Qiu, Z. Wang, H. Zhao, K. Qin, Z. Li, and H. Hu, “Inertial/magnetic sensors based pedestrian dead reckoning by means of multi-sensor fusion,” *Inf. Fusion*, vol. 39, pp. 108–119, 2018.

[34] F. Carneiro, R. Tavares, J. Rodrigues, P. Abreu, and M. T. Restivo, “A gamified approach for hand rehabilitation device,” *Int. J. Online Eng.*, vol. 14, no. 1, pp. 179–186, 2018.

[35] S. Zhou, F. Fei, G. Zhang, Y. Liu, and W. J. Li, “Hand-writing motion tracking with vision-inertial sensor fusion: Calibration and error correction,” *Sensors (Switzerland)*, vol. 14, no. 9, pp. 15641–15657, 2014.

[36] P. Zhou, M. Li, and G. Shen, “Use It Free: Instantly Knowing Your Phone Attitude,” *Mobicom’14*, pp. 605–616, 2014.

[37] R. Mahony, T. Hamel, J.-M. M. Pflimlin, and R. Mahony, “Nonlinear Complementary Filters on the Special Orthogonal Group,” *IEEE Trans. Automat. Contr.*, vol. 53, no. 5, pp. 1203–1217, 2008.

[38] S. O. H. Madgwick, “An efficient orientation filter for inertial and inertial/magnetic sensor arrays,” *Report x-io and University of Bristol (UK)*, 2010. [Online].

Available: https://www.samba.org/tridge/UAV/madgwick_internal_report.pdf. [Accessed: 01-May-2018].

[39] P. Daponte, L. De Vito, M. Riccio, and C. Sementa, “Design and validation of a motion-tracking system for ROM measurements in home rehabilitation,” *Meas. J. Int. Meas. Confed.*, vol. 55, pp. 82–96, 2014.

[40] A. Hadjidj, M. Souil, A. Bouabdallah, Y. Challal, and H. Owen, “Wireless sensor networks for rehabilitation applications: Challenges and opportunities,” *J. Netw. Comput. Appl.*, vol. 36, no. 1, pp. 1–15, 2013.

[41] M. Biagi, A. M. Vegni, and T. D. C. C. Little, “LAT indoor MIMO-VLC Localize, access and transmit,” *2012 Int. Work. Opt. Wirel. Commun. IWOW 2012*, no. 1, 2012.

[42] Y. Li, M. Safari, R. Henderson, and H. Haas, “Optical OFDM With Single-Photon Avalanche Diode,” *IEEE Photonics Technol. Lett.*, vol. 27, no. 9, pp. 943–946, 2015.

[43] S. Hann, J. H. Kim, S. Y. Jung, and C. S. Park, “White LED ceiling lights positioning systems for optical wireless indoor applications,” *Eur. Conf. Opt. Commun. ECOC*, vol. 1–2, no. 0, pp. 2–4, 2010.

[44] S.-Y. Jung, “OPTICAL WIRELESS INDOOR POSITIONING SYSTEM USING LIGHT EMITTING DIODE CEILING LIGHTS,” *Microw. Opt. Technol. Lett.*, vol. 54, no. 12, pp. 2781–2784, 2012.

[45] S. Y. Jung, S. Hann, and C. S. Park, “TDOA-based optical wireless indoor localization using LED ceiling lamps,” *IEEE Trans. Consum. Electron.*, vol. 57, no.

4, pp. 1592–1597, 2011.

[46] Z. Zhou, “Indoor positioning algorithm using light-emitting diode visible light communications,” *Opt. Eng.*, vol. 51, no. 8, p. 085009, 2012.

[47] S. H. Yang, H. S. Kim, Y. H. Son, and S. K. Han, “Three-dimensional visible light indoor localization using AOA and RSS with multiple optical receivers,” *J. Light. Technol.*, vol. 32, no. 14, pp. 2480–2485, 2014.

[48] E. Jeong, D. Kim, S. Yang, H. Kim, Y. Son, and S. Han, “Estimated Position Error Compensation in Localization Using Visible Light Communication,” *IEEE Int. Conf. ubiquitous Futur. networks*, pp. 470–471, 2013.

[49] E. Jeong, S. Yang, H. Kim, and S. Han, “Tilted receiver angle error compensated indoor positioning system based on visible light communication,” *Electron. Lett.*, vol. 49, no. 14, pp. 4–5, 2013.

[50] M. Yasir, S. Ho, B. N. Vellambi, S. Member, S. Ho, and B. N. Vellambi, “Indoor Positioning System Using Visible Light and Accelerometer,” *J. Light. Technol.*, vol. 32, no. 19, pp. 3306–3316, 2014.

[51] M. Yasir, S.-W. Ho, and B. N. Vellambi, “Indoor position tracking using multiple optical receivers,” *J. Light. Technol.*, vol. 34, no. 4, pp. 1166–1176, 2016.

[52] J. Vongkulbhisal, “A FINGERPRINTING-BASED INDOOR LOCALIZATION SYSTEM USING INTENSITY MODULATION OF LIGHT EMITTING,” *CEUR Workshop Proc.*, vol. 1594, no. 5, pp. 74–79, 2012.

[53] Y.-Y. Won, S.-K. Han, D.-H. Kim, and S.-H. Yang, “Three-dimensional optical wireless indoor positioning system using location code map based on power

distribution of visible light emitting diode," *IET Optoelectron.*, vol. 7, no. 3, pp. 77–83, 2013.

[54] J. Lui, A. M. Vegni, L. Colace, A. Neri, and C. Menon, "Preliminary design and characterization of a low-cost and low-power visible light positioning system," *Appl. Opt.*, 2018.

[55] R. F. Brena, J. P. García-Vázquez, C. E. Galván-Tejada, D. Muñoz-Rodriguez, C. Vargas-Rosales, and J. Fangmeyer, "Evolution of Indoor Positioning Technologies: A Survey," *J. Sensors*, vol. 2017, 2017.

[56] M. Shankar, J. B. Burchett, Q. Hao, B. D. Guenther, and D. J. Brady, "Human-tracking systems using pyroelectric infrared detectors," *Opt. Eng.*, vol. 45, no. 10, p. 106401, 2006.

[57] G. Ding *et al.*, "Spectral characteristic of infrared radiations of some acupoint and non-acupoint areas in human arm surface," *Chinese Sci. Bull.*, vol. 46, no. 8, pp. 678–682, 2001.

[58] M. Kohli *et al.*, "Pyroelectric thin-film sensor array," *Sensors Actuators A Phys.*, vol. 60, no. 1–3, pp. 147–153, 1997.

[59] Omron, "Omron D6T MEMS Thermal Sensors." .

[60] Glolab, "How Infrared Motion Detector Components Work." [Online]. Available: http://www.glolab.com/pirparts/infrared.html. [Accessed: 16-Jun-2019].

[61] M. J. Mathie, A. C. F. Coster, N. H. Lovell, and B. G. Celler, "Accelerometry: Providing an integrated, practical method for long-term, ambulatory monitoring of human movement," *Physiol. Meas.*, vol. 25, no. 2, pp. 1–20, 2004.

[62] F. R. Allen, E. Ambikairajah, N. H. Lovell, and B. G. Celler, “Classification of a known sequence of motions and postures from accelerometry data using adapted Gaussian mixture models,” *Physiol. Meas.*, vol. 27, no. 10, pp. 935–951, 2006.

[63] Z. Zhang, L. Liparulo, M. Panella, X. Gu, and Q. Fang, “A Fuzzy Kernel Motion Classifier for Autonomous Stroke Rehabilitation,” *IEEE J. Biomed. Heal. Informatics*, vol. 20, no. 3, pp. 893–901, 2016.

[64] Q. Xu and S. Hranilovic, “IDyLL : Indoor Localization using Inertial and Light Sensors on Smartphones,” no. September, 2015.

[65] T. Hester *et al.*, “Using wearable sensors to measure motor abilities following stroke,” *Int. Work. Wearable Implant. Body Sens. Networks*, pp. 1–4, 2006.

[66] J. Yang, “Toward Physical Activity Diary: Motion Recognition Using Simple Acceleration Features with Mobile Phones,” *Proc. 1st Int. Work. Interact. Multimed. Consum. Electron.*, pp. 1–10, 2009.

[67] F. Foerster, M. Smeja, and J. Fahrenberg, “Detection of posture and motion by accelerometry : a validation study in ambulatory monitoring,” vol. 15, no. 5, pp. 571–583, 1999.

[68] H. Zhou, T. Stone, H. Hu, and N. Harris, “Use of multiple wearable inertial sensors in upper limb motion tracking,” *Med. Eng. Phys.*, vol. 30, no. 1, pp. 123–133, 2008.

[69] R. DeVaul and S. Dunn, “Real-time motion classification for wearable computing applications,” *Mit*, pp. 1–14, 2001.

[70] L. Bao and S. S. Intille, “Activity Recognition from User-Annotated Acceleration

Data," *Pervasive Comput.*, vol. 3001, pp. 287–304, 2004.

[71] K. Aminian, P. Robert, E. E. Buchser, B. Rutschmann, D. Hayoz, and M. Depairon, "Physical activity monitoring based on accelerometry: Validation and comparison with video observation," *Med. Biol. Eng. Comput.*, vol. 37, no. 3, pp. 304–308, 1999.

[72] C. Bishop, *Pattern Recognition and Machine Learning*, vol. 4, no. 356. 2006.

[73] T. Imam, K. Ting, and J. Kamruzzaman, "z-SVM: An SVM for Improved Classification of Imbalanced Data BT - AI 2006: Advances in Artificial Intelligence," pp. 264–273, 2006.

[74] D. Roetenberg, H. Luinge, and P. Slycke, "Xsens MVN: Full 6DOF Human Motion Tracking Using Miniature Inertial Sensors," vol. 3, 2013.

[75] A. Zinnen, U. Blanke, and B. Schiele, "An analysis of sensor-oriented vs. model-based activity recognition," *Int. Symp. Wearable Comput.*, pp. 93–100, 2009.

[76] Z. Zhang, Q. Fang, and F. Ferry, "Upper limb motion capturing and classification for unsupervised stroke rehabilitation," in *Industrial Electronics Conference*, 2011, pp. 3832–3836.

[77] J. Craig, *Introduction to Robotics*, vol. 1, no. 2. 1986.

[78] M. Zhang and A. A. Sawchuk, "Human daily activity recognition with sparse representation using wearable sensors," *IEEE J. Biomed. Heal. Informatics*, vol. 17, no. 3, pp. 553–560, 2013.

[79] A. M. Khan, Y. K. Lee, S. Y. Lee, and T. S. Kim, "A triaxial accelerometer-based

physical-activity recognition via augmented-signal features and a hierarchical recognizer," *IEEE Trans. Inf. Technol. Biomed.*, vol. 14, no. 5, pp. 1166–1172, 2010.

[80] N. Ravi, N. Dandekar, P. Mysore, and M. Littman, "Activity recognition from accelerometer data," *Am. Assoc. Artif. Intell.*, vol. 5, pp. 1541–1546, 2005.

[81] M. Tseng, K. Liu, C. Hsieh, S. J. Hsu, and C. Chan, "Gesture spotting algorithm for door opening using single wearable sensor," in *IEEE International Conference on Applied System Invention*, 2018, pp. 854–856.

[82] M. Panwar *et al.*, "CNN based approach for activity recognition using a wrist-worn accelerometer," in *Proceedings of the Annual International Conference of the IEEE Engineering in Medicine and Biology Society, EMBS*, 2017, pp. 2438–2441.

[83] D. Biswas *et al.*, "Recognition of elementary arm movements using orientation of a tri-axial accelerometer located near the wrist," *Physiol. Meas.*, vol. 35, no. 9, pp. 1751–1768, 2014.

[84] J. Yang, J. Wang, and Y. Chen, "Using acceleration measurements for activity recognition : An effective learning algorithm for constructing neural classifiers," *Pattern Recognit. Lett.*, vol. 29, no. 16, pp. 2213–2220, 2008.

[85] G. Bauer, U. Blanke, P. Lukowicz, and B. Schiele, "User independent, multi-modal spotting of subtle arm actions with minimal training data," *2013 IEEE Int. Conf. Pervasive Comput. Commun. Work. PerCom Work. 2013*, no. March, pp. 8–13, 2013.

[86] Seon-Woo Lee and K. Mase, "Recognition of walking behaviors for pedestrian

navigation," no. January, pp. 1152–1155, 2002.

[87] J. Yun and S.-S. Lee, "Human movement detection and identification using pyroelectric infrared sensors.," *Sensors (Basel).*, vol. 14, no. 5, pp. 8057–81, 2014.

[88] Q. Hao, D. J. Brady, B. D. Guenther, J. B. Burchett, M. Shankar, and S. Feller, "Human tracking with wireless distributed pyroelectric sensors," *IEEE Sens. J.*, vol. 6, no. 6, pp. 1683–1695, 2006.

[89] B. Yang, J. Luo, and Q. Liu, "A novel low-cost and small-size human tracking system with pyroelectric infrared sensor mesh network," *Infrared Phys. Technol.*, vol. 63, pp. 147–156, 2014.

[90] J. Lui, A. Ferrone, K. Andrews, L. Colace, and C. Menon, "A preliminary investigation into infrared sensors in wearables for upper extremity motion sensing," in *Future Technologies Conference*, 2017, no. November, pp. 120–125.

[91] InvenSense, "MPU9250 Product Specification Revision 1.1," 2016. [Online]. Available: https://www.invensense.com/wp-content/uploads/2015/02/PS-MPU-9250A-01-v1.1.pdf. [Accessed: 01-May-2018].

[92] Omron, "Omron D6T MEMS Thermal Sensors." [Online]. Available: https://omronfs.omron.com/en_US/ecb/products/pdf/en-d6t.pdf. [Accessed: 01-May-2018].

[93] OMRON, "OMRON D6T MEMS Datasheet." pp. 1–4.

[94] J. Y. Lee, S. Y. Kwon, W. S. Kim, S. J. Hahn, J. Park, and N. J. Paik, "Feasibility, reliability, and validity of using accelerometers to measure physical activities of

patients with stroke during inpatient rehabilitation," *PLoS One*, vol. 13, no. 12, pp. 1–13, 2018.

[95] L. A. Simpson, J. J. Eng, and M. Chan, "H-GRASP: the feasibility of an upper limb home exercise program monitored by phone for individuals post stroke," *Disabil. Rehabil.*, vol. 39, no. 9, pp. 874–882, 2017.

[96] J. Eng and J. Harris, "Graded Repetitive Arm Supplementary Program: A home-work based program to improve arm and hand function in people living with stroke," 2012. [Online]. Available: https://neurorehab.med.ubc.ca/files/2013/06/GRASP-Instruction-Manual.pdf. [Accessed: 01-Jan-2018].

[97] B. D. Mowery, "The Paired t -Test," *Pediatr. Nurs.*, vol. 37, no. 6, pp. 320–322, 2011.

[98] I. González, J. Fontecha, R. Hervás, and J. Bravo, "An Ambulatory System for Gait Monitoring Based on Wireless Sensorized Insoles," *Sensors*, vol. 15, no. 7, pp. 16589–16613, 2015.

[99] D. Biswas *et al.*, "Recognizing upper limb movements with wrist worn inertial sensors using k-means clustering classification," *Hum. Mov. Sci.*, vol. 40, pp. 59–76, 2015.

[100] J. Lui and C. Menon, "Would a thermal sensor improve arm motion classification accuracy of a single wrist-mounted inertial device?," *Biomed. Eng. Online*, vol. 18, no. 1, pp. 1–17, 2019.

[101] L. Gao, A. K. Bourke, and J. Nelson, "Evaluation of accelerometer based multi-

sensor versus single-sensor activity recognition systems," *Med. Eng. Phys.*, vol. 36, no. 6, pp. 779–785, 2014.

[102] A. Krause *et al.*, "Trading off prediction accuracy and power consumption for context-aware wearable computing," in *IEEE International Symposium on Wearable Computers, ISWC*, 2005, pp. 20–26.

[103] C. L. Massie, M. P. Malcolm, D. P. Greene, and R. C. Browning, "Kinematic motion analysis and muscle activation patterns of continuous reaching in survivors of stroke," *J. Mot. Behav.*, vol. 44, no. 3, pp. 213–222, 2012.

[104] S. E. Fasoli, H. I. Krebs, J. Stein, W. R. Frontera, and N. Hogan, "Effects of robotic therapy on motor impairment and recovery in chronic stroke," *Arch. Phys. Med. Rehabil.*, vol. 84, no. 4, pp. 477–482, 2003.

[105] R. Tavares, P. Abreu, and M. T. Restivo, "An online collaborative environment for rehabilitation using instrumented devices," in *Experiment@ International Conference*, 2017, pp. 95–96.

[106] V. F. Bento, V. T. Cruz, D. D. Ribeiro, M. M. Colunas, and J. P. S. Cunha, "The SWORD tele-rehabilitation system," *Stud. Health Technol. Inform.*, vol. 177, pp. 76–81, 2012.

[107] Omron, "D6T MEMS Thermal Sensors User's Manual." [Online]. Available: https://omronfs.omron.com/en_US/ecb/products/pdf/en_D6T_users_manual.pdf.

[108] Sharp, "Sharp GP2Y0A21YK (10cm-80cm)," 1968. [Online]. Available: https://www.sparkfun.com/datasheets/Components/GP2Y0A21YK.pdf.

[109] Sharp, "Sharp GP2Y0A51SK (2cm-15cm)." [Online]. Available: http://www.sharp-

world.com/products/device/lineup/data/pdf/datasheet/gp2y0a51sk_e.pdf.

[110] Adafruit, “Adafruit LSM9DS0 Accelerometer + Gyro + Magnetometer 9-DOF Breakouts,” 2014. [Online]. Available: https://cdn-learn.adafruit.com/downloads/pdf/adafruit-lsm9ds0-accelerometer-gyro-magnetometer-9-dof-breakouts.pdf?timestamp=1565461337.

Appendix A.

Contributions

A list of publications that have been accepted, or submitted, as a result of the work associated with this thesis is provided below.

Published/Accepted Refereed Journal Papers

1. Lui J, Menon C. Would a thermal sensor improve arm motion classification accuracy of a single wrist-mounted inertial device?. Biomedical engineering online. 2019 Dec;18(1):53.

2. Lui, J, Vegni AM, Colace L, Menon C, Neri A. Preliminary design and characterization of a low-cost and low-power visible light positioning system., Applied Optics, 2018

Published/Accepted Refereed Conference Extended Abstracts

1. Lui J, Andrews K, Ferrone A, Colace L, Menon C. A preliminary investigation into infrared sensors in wearables for upper extremity motion sensing.

2. Lui J, Ferrone A, Lim ZY, Colace L, Menon C. A Novel Wearable for Rehabilitation Using Infrared Sensors: A Preliminary Investigation. In International Conference on Bioinformatics and Biomedical Engineering 2017 Apr 26 (pp. 573-583). Springer, Cham.

Appendix B.

Preliminary Analysis and Results from prior work

The following figures and tables result from an analysis of prior investigations and informed the hardware choices in the current thesis. The sensor hardware descriptions are first summarized in Table 7.1.

Table 7.1. Sensor hardware descriptions

Sensor Number in Figure 3.1	Sensor Short name	Sensor Description	Sensor Model
1	Omron 16-1	16-element PIR. Mounted proximal, oriented upward	Omron D6T-44L, Omron Corporation, [107]
2	Omron 16-2	16-element PIR. Mounted proximal, oriented downward	Omron D6T-L, Omron Corporation, [107]
3	Short Distance 1	16-element PIR. Mounted proximal, oriented upward	Omron D6T-8L, Omron Corporation, [107]
4	Short Distance 2	16-element PIR. Mounted proximal, oriented downward	Omron D6T-8L, Omron Corporation, [107]
5	Long Distance 1	IR Distance sensor, oriented upward	GP2Y0A21YK, Sharp, [108]
6	Long Distance 2	IR Distance sensor, oriented downward	GP2Y0A21YK, Sharp, [108]
7	Omron 8-1	IR Distance sensor, oriented upward	GP2Y0A51SK, Sharp, [109]
8	Omron 8-2	IR Distance sensor, oriented downward	GP2Y0A51SK, Sharp, [109]
9	Accelerometer	Accelerometer sensor	LSM9DS0, Adafruit, [110]
9	Gyroscope	Gyroscope sensor	LSM9DS0, Adafruit, [110]

Analysis of the classifier performance for each of the sensor data indicated that the more proximal and downward oriented 16-element array PIR sensor delivered the highest individual classification accuracy of any sensor, Figure 7.1 and in Table 7.2.

Table 7.2. Classification performance of single sensors

Sensor	Classification Accuracy
Omron 16-2 “Downward”	45%
Omron 16-1 “Upward”	38%
Omron 8-2 “Downward”	24%
Omron 8-1 “Upward”	23%
Acc	19%
Long Distance 2	16%
Long Distance 1	12%
Short Distance 2	10%
Short Distance 1	9%
Gyro	7%

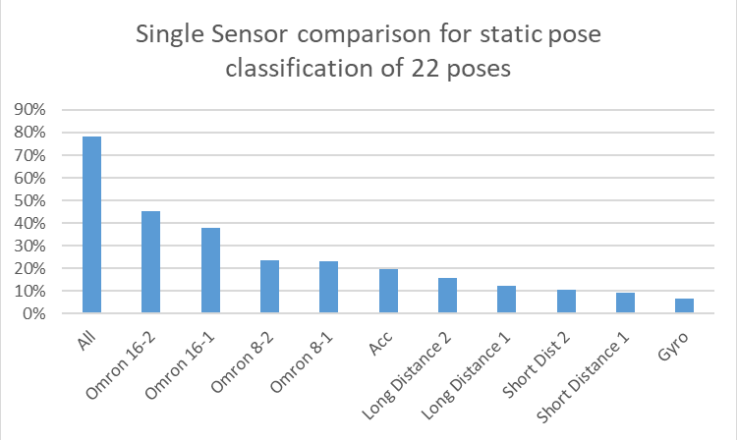

Figure 7.1. Static pose classification accuracy for each of the sensors

The classification matrix for the upper pointing 16-element thermal sensor, Figure 7.3, provides comparable but slightly lower classification accuracy (45% vs 38% accuracy) than the downward pointing PIR sensor, Figure 7.2. The increased classification accuracy of the downward-pointing sensor might result from increased visibility of the user in the downward sensor, while the upward pointing sensor, which is oriented toward the user’s head, might have fewer pixels ‘lit-up’ by the smaller target. The upper sensor will point

upwards toward the user's shoulders and head and will see less of the user during poses compared to the lower sensor, which is oriented toward the user's torso. Comparing the confusion matrices of the two sensors may verify this hypothesis (Figure 7.2, Figure 7.3), as the forward reaching motions are classified more accurately with the downward oriented sensor, whereas the performance of the upward sensor degrades at 15 – 30 cm and 50 cm distances.

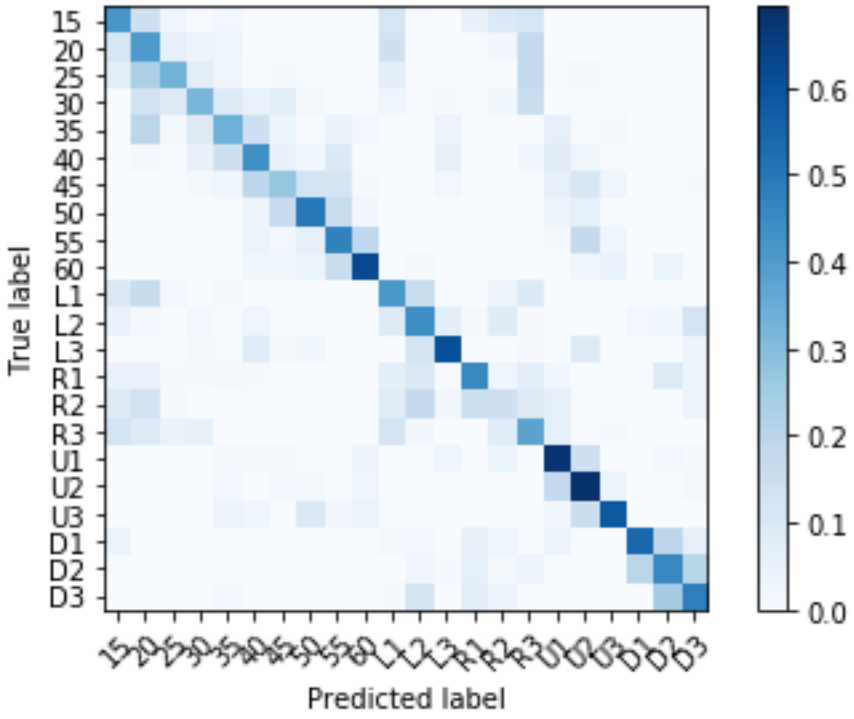

Figure 7.2. Confusion matrix for Downward proximal 16-element PIR sensor – "Omron 16-2"

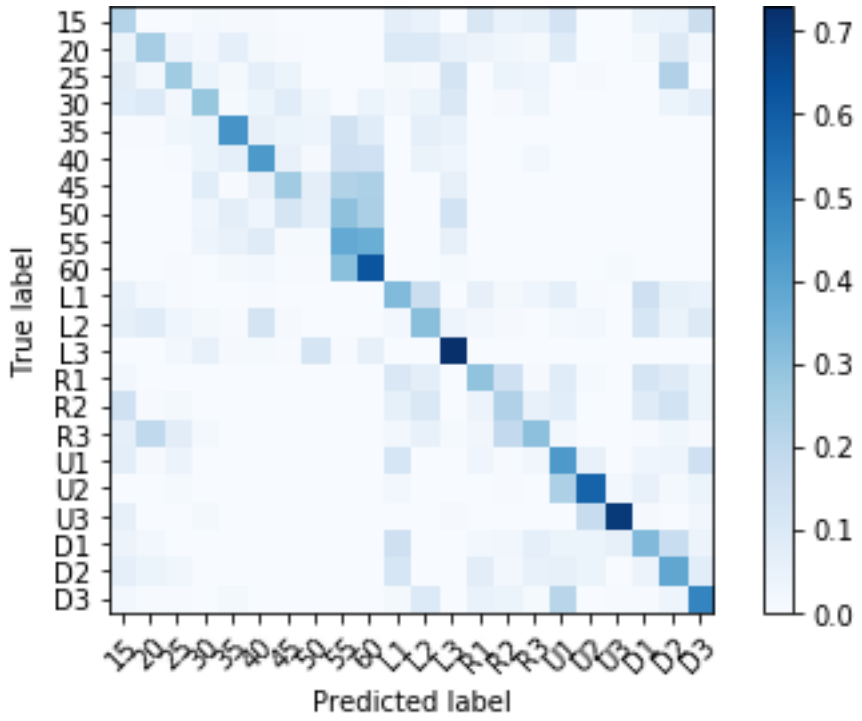

Figure 7.3. Confusion matrix for Upward proximal 16-element PIR sensor "Omron 16-1"

The distal thermal sensors also provide some considerable classification accuracy that is higher than the accelerometer sensor, Table 7.2. It is possible that the thermal sensors at any of these 4 orientations on the prototype device provide more insight into the static pose of the user's arm than the accelerometer can provide, since the raw data from accelerometer is essentially a tilt sensor, and tilt angles measured at the wrist are insufficient for reconstructing pose of the human body. A confusion matrix of accelerometer predictions is shown in Figure 7.4. It can be observed that the classifier performs well primarily for upward and downward reaching actions, indicating that the raw accelerometer data is primarily useful for distinguishing poses as they differ with elevation angle relative to the horizon.

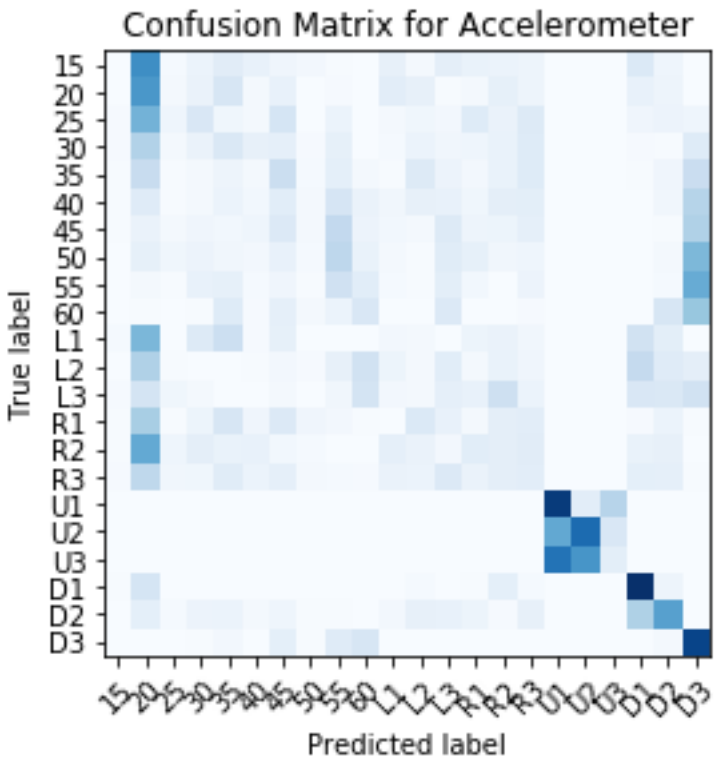

Figure 7.4. Confusion Matrix for accelerometer

Adding gyroscope and orientation does not significantly increase the performance of accelerometer, except for a possible increase in left and right reaching motion accuracy, Figure 7.5.

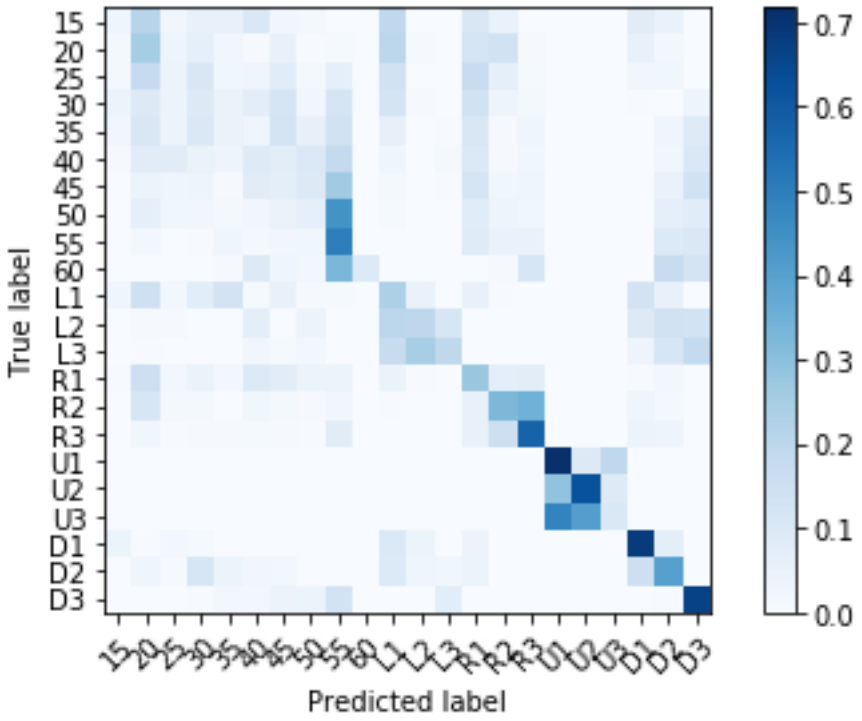

Figure 7.5. Confusion matrix for accelerometer, gyroscope, and orientation

The IR distance sensors provide a poor determination of pose, Figure 7.6. Perhaps the strongest performance of the distance sensors is reported in differentiating left, right, up, and down reaching motions. This may indicate that the distance sensors could provide some useful guidance in sensing distance from user to nearby stationary objects such as tables and walls, but this might not provide strong enough insight into differentiating multiple complex poses or actions along a single axis of movement. For example, the classification performance for different forward reaching motions is very poor.

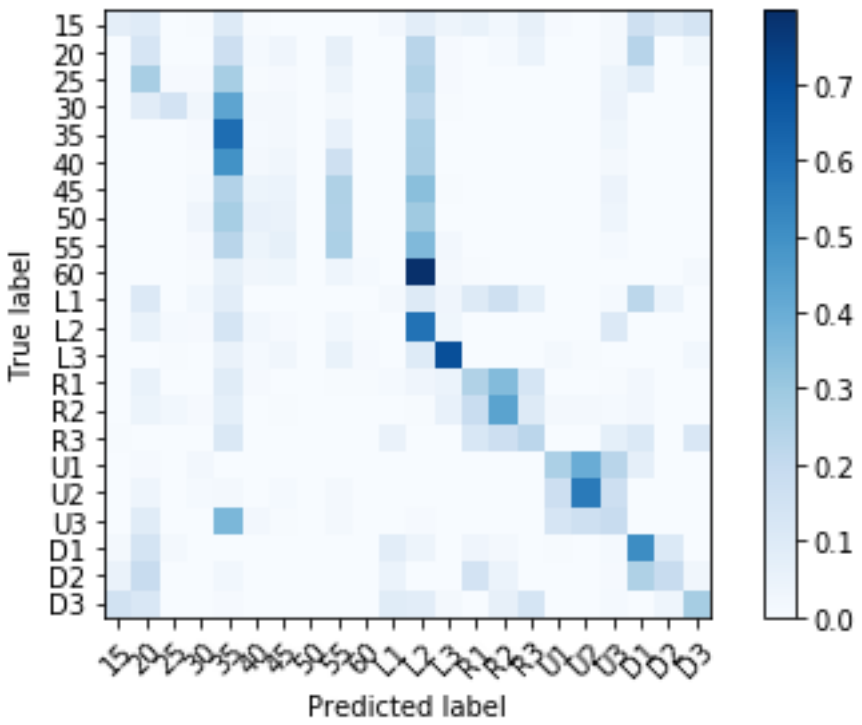

Figure 7.6. Confusion matrix for IR Distance sensors

Combining all PIR thermal sensors provides a strong classifier performance, Figure 7.7. The thermal sensor provides stronger classification accuracy than the accelerometer for poses across different axes, especially for movements reaching to the left, right, and downwards. The accelerometer, in contrast, is unable to provide strong prediction accuracy in these axes, and primarily delivers strong predictions for motions upward and downward, since the raw accelerometer sensor primarily provides insight into orientation and tilting of the limb.

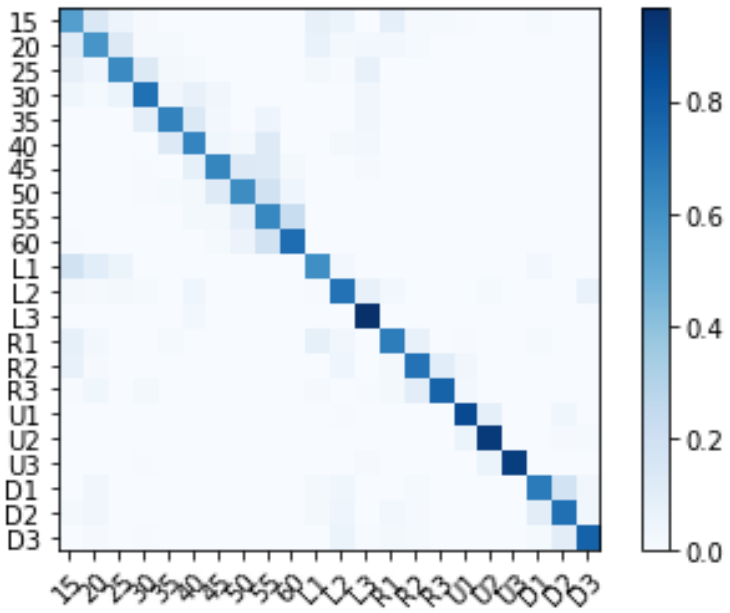

Figure 7.7. Confusion matrix for Four PIR sensors

Appendix C.

Microcontroller Software code

```
#include "quaternionFilters.h"
#include "MPU9250.h"
#include <Wire.h>
#include <SoftwareSerial.h>
#include <WireExt.h>

// CUSTOMIZABLE CONFIG
// Modify this content as needed
#define sendThermalFreq 5 // Send Omron at 1/5 rate of the IMU data. Set to 0 or -1 if we
want to transmit in regular setup.
// Bluetooth settings
int bluetoothTx = 2;  // TX-O pin of bluetooth mate, Arduino D2
int bluetoothRx = 3;  // RX-I pin of bluetooth mate, Arduino D3

// OTHER CONFIG
#define D6T_addr 0x0A // 7 bit address of OMRON D6T is 0x0A in hex, 0000 1010 in binary
#define D6T_cmd 0x4C // Standard command is 4C in hex, 0100 1100 in binary

// Initialize
SoftwareSerial bluetooth(bluetoothTx, bluetoothRx);
MPU9250 myIMU;

// Initialize global variables
int outputCount = 0; // Counter to increment in between IMU and Thermal sensor
acquisitions
unsigned int deltaTime = 0; // Time stamp
int rbuf[35]; // Actual raw data is coming in as 35 bytes for OMRON 4x4
unsigned int tdata[16]; // Thermal sensor requires 16 element vector
unsigned char tdatashift[16];
unsigned int t_PTAT;
int i = 0;

// Set up the arrays that we receive IMU data into
unsigned int acceldata[3];
unsigned int gyrodata[3];
float quat[4];
unsigned int quatshift[4];

// Set up char array to store the high and low bytes for each sensor
unsigned char temphighbyte[16];
unsigned char templowbyte[16];
unsigned char accelhighbyte[3];
unsigned char accellowbyte[3];
unsigned char gyrohighbyte[3];
unsigned char gyrolowbyte[3];
unsigned char quathighbyte[4];
unsigned char quatlowbyte[4];

float magCalibration[3] = {0, 0, 0}, magbias[3] = {0, 0, 0};  // Factory mag calibration
and mag bias
float gyroBias[3] = {0, 0, 0}, accelBias[3] = {0, 0, 0};      // Bias corrections for
gyro and accelerometer

void setup()
{
  Wire.begin();
  bluetooth.begin(115200);  // The Bluetooth Mate defaults to 115200bps
  delay(100);  // Short delay, wait for the Mate to send back CMD
  myIMU.initMPU9250();
  myIMU.initAK8963(myIMU.magCalibration);
}
```

```
void loop()
{
  outputCount++;
  if (outputCount == sendThermalFreq) // If outputCount == sendThermalFreq, then we read
thermal sensor and transmit
  {
    // Read the Omron data
    readOmron();
    getBytes();

    // Send over bluetooth
    sendBluetooth();
    // Reset the outputCount so that we resume IMU reading
    outputCount = 0;
  }
  else // Otherwise we read from IMU and transmit
  {
    // Read from IMU
    readIMU();
    // Convert to single byte data
    getBytes();
    // Send IMU data
    sendIMU();
  }
}

void sendIMU()
{
  // Send IMU data
  for (i = 0; i < 3; i++)
  {
    bluetooth.write(accelhighbyte[i]);
    bluetooth.write(accellowbyte[i]);
  }
  for (i = 0; i < 3; i++)
  {
    bluetooth.write(gyrohighbyte[i]);
    bluetooth.write(gyrolowbyte[i]);
  }
  for (i = 0; i < 4; i++)
  {
    bluetooth.write(quathighbyte[i]);
    bluetooth.write(quatlowbyte[i]);
  }
  deltaTime = millis();
  bluetooth.write(highByte(deltaTime));
  bluetooth.write(lowByte(deltaTime));
  bluetooth.write('\n');
}

void sendBluetooth()
{
  for (i = 0; i < 16; i++)
      {
        bluetooth.write(tdatashift[i]);
      }
  bluetooth.write('\n');
}

void readOmron()
{
  Wire.beginTransmission(D6T_addr);
  Wire.write(D6T_cmd);
  Wire.endTransmission();
  delay(1);
  if (WireExt.beginReception(D6T_addr) >= 0)
  {
    i = 0;
    for (i = 0; i < 35; i++)
    {
      rbuf[i] = WireExt.get_byte();
```

```
    }
    WireExt.endReception(); // End reception
    t_PTAT = (rbuf[0] + (rbuf[1] << 8));
    // Calculate the individual element values
    for (i = 0; i < 16; i++) {
      tdata[i] = (rbuf[(i * 2 + 2)] + (rbuf[(i * 2 + 3)] << 8));

    }
  } // if (WireExt.beginReception(D6T_addr) >= 0)

  // shift our data so we can transmit with 8 bit int. Output is written into tdatashift
  scaleThermal(tdata,150,405);

} // readOmron()

void scaleThermal(int dataArray[], int low, int high)
{
  // Scale the thermal sensor data in a range that that fits in a 8 bit (1 byte) char
  // Example scaling from 405 - 150 covers a realistic temperature range and allows 1
byte storage
  for (int i = 0; i < 16; i++)
  {
    if (dataArray[i] > high) // 405 max temp
    {
      dataArray[i] = high - low;
    }
    else if (dataArray[i] < low) //
    {
      dataArray[i] = 0;
    }
    else
    {
      dataArray[i] = dataArray[i] - low;
    }
  }
}

void readIMU()
{
  // Read the x/y/z adc values
  myIMU.readAccelData(myIMU.accelCount);
  myIMU.getAres();
  // Now we'll calculate the accleration value into actual g's
  // This depends on scale being set
  myIMU.ax = ((float)myIMU.accelCount[0] * myIMU.aRes) - 0.14; // - accelBias[0];
  myIMU.ay = ((float)myIMU.accelCount[1] * myIMU.aRes) - 0.06; // - accelBias[1];
  myIMU.az = ((float)myIMU.accelCount[2] * myIMU.aRes) + 0.17; // - accelBias[2];

  acceldata[0] =  (myIMU.ax) * 100 + 800;
  acceldata[1] =  (myIMU.ay) * 100 + 800;
  acceldata[2] =  (myIMU.az) * 100 + 800;

  // Read the x/y/z adc values
  myIMU.readGyroData(myIMU.gyroCount);
  myIMU.getGres();
  // Calculate the gyro value into actual degrees per second
  // This depends on scale being set
  myIMU.gx = ((float)myIMU.gyroCount[0] * myIMU.gRes) + 1;
  myIMU.gy = ((float)myIMU.gyroCount[1] * myIMU.gRes) - 2;
  myIMU.gz = ((float)myIMU.gyroCount[2] * myIMU.gRes) - 0.3;

  gyrodata[0] =  (myIMU.gx) * 10 + 32500;
  gyrodata[1] =  (myIMU.gy) * 10 + 32500;
  gyrodata[2] =  (myIMU.gz) * 10 + 32500;

  myIMU.readMagData(myIMU.magCount);  // Read the x/y/z adc values
  myIMU.getMres();
  // User environmental x-axis correction in milliGauss, should be
  // automatically calculated
  magbias[0] = +470.;
  // User environmental x-axis correction in milliGauss TODO axis??
```

```
  magbias[1] = +120.;
  // User environmental x-axis correction in milliGauss
  magbias[2] = +125.;

  // Calculate the magnetometer values in milliGauss
  // Include factory calibration per data sheet and user environmental
  // corrections
  // Get actual magnetometer value, this depends on scale being set
  myIMU.mx = (float)myIMU.magCount[0] * myIMU.mRes * myIMU.magCalibration[0] - magbias[0];
  myIMU.my = (float)myIMU.magCount[1] * myIMU.mRes * myIMU.magCalibration[1] - magbias[1];
  myIMU.mz = (float)myIMU.magCount[2] * myIMU.mRes * myIMU.magCalibration[2] - magbias[2];

  myIMU.updateTime();
  MahonyQuaternionUpdate(myIMU.ax, myIMU.ay, myIMU.az, myIMU.gx * DEG_TO_RAD,
                         myIMU.gy * DEG_TO_RAD, myIMU.gz * DEG_TO_RAD, myIMU.my,
                         myIMU.mx, myIMU.mz, myIMU.deltat);

  // Update and format quaternion values
  quat[0] = *getQ();
  quat[1] = *(getQ() + 1);
  quat[2] = *(getQ() + 2);
  quat[3] = *(getQ() + 3);
  quatshift[0] = quat[0] * 100 + 800;
  quatshift[1] = quat[1] * 100 + 800;
  quatshift[2] = quat[2] * 100 + 800;
  quatshift[3] = quat[3] * 100 + 800;
} // readIMU()
```

```
void getBytes()
{
  // Prepare sensor data for transmission
  // Split the sensor data into high byte and low byte arrays
  // Thermal sensor data
  for (i = 0; i < 16; i++)
  {
    if (tdatashift[i] == 0xA)
    {
      tdatashift[i] = 0xB;
    }
  }
  // Accelerometer data
  for (i = 0; i < 3; i++)
  {
    accelhighbyte[i] = highByte(acceldata[i]);
    accellowbyte[i] = lowByte(acceldata[i]);

    if (accelhighbyte[i] == 0xA)
    {
      accelhighbyte[i] = 0xB;
    }
    if (accelhighbyte[i] == 0xA)
    {
      accellowbyte[i] = 0xB;
    }
  }// Accelerometer loop

  // Gyroscope data
  for (i = 0; i < 3; i++)
  {
    gyrohighbyte[i] = highByte(gyrodata[i]);
    gyrolowbyte[i] = lowByte(gyrodata[i]);

    if (gyrohighbyte[i] == 0xA)
    {
      gyrohighbyte[i] = 0xB;
    }
    if (gyrohighbyte[i] == 0xA)
    {
      gyrolowbyte[i] = 0xB;
    }
  } // Gyro loop

  // Quaternion data
  for (i = 0; i < 4; i++)
  {
    quathighbyte[i] = highByte(quatshift[i]);
    quatlowbyte[i] = lowByte(quatshift[i]);

    if (quathighbyte[i] == 0xA)
    {
      quathighbyte[i] = 0xB;
    }
    if (quathighbyte[i] == 0xA)
    {
      quatlowbyte[i] = 0xB;
    }

  } // Quaternion loop
} // getBytes()
```